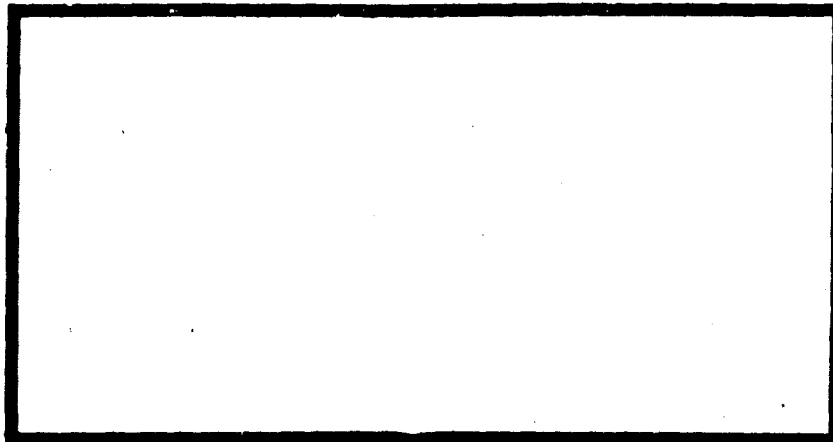
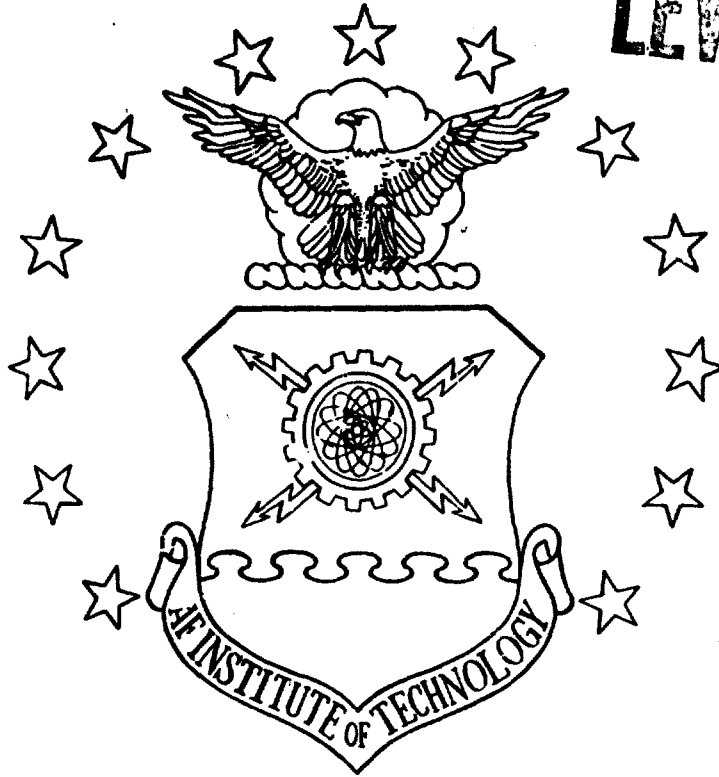


DDC

LEVEL *it*



AD A100870



DTIC FILE COPY

DTIC
SELECTE
JUL 2 1981
S D

UNITED STATES AIR FORCE
AIR UNIVERSITY
AIR FORCE INSTITUTE OF TECHNOLOGY
Wright-Patterson Air Force Base, Ohio

A

This document has been approved for public release and sale; its distribution is unlimited.

THIS DOCUMENT TO BEST QUALITY PRACTICABLE. THE COPY FURNISHED TO DDC CONTAINED A SIGNIFICANT NUMBER OF PAGES WHICH DO NOT REPRODUCE LEGIBLY.

81 6 30 073

DISCLAIMER NOTICE

**THIS DOCUMENT IS BEST QUALITY
PRACTICABLE. THE COPY FURNISHED
TO DTIC CONTAINED A SIGNIFICANT
NUMBER OF PAGES WHICH DO NOT
REPRODUCE LEGIBLY.**

6
ADAPTIVE LASER POINTING
AND
TRACKING PROBLEM

7
Master's THESIS

Presented to the Faculty of the School of Engineering
of the Air Force Institute of Technology
Air University
in Partial Fulfillment of the
Requirements for the Degree of
Master of Science in Electrical Engineering

12 / 112

by
10 James Singletery, Jr B.S.E.E.
1st Lt USAF

Graduate Electro-Optics

11 December 1980

Administrative stamp with handwritten 'A 230' and a signature.

Approved for public release; distribution unlimited.

012225

Yur

Preface

This report is the third in a series of research projects devoted to the development of an extended Kalman filter algorithm for use in a ground based laser system located at Kirtland AFB, New Mexico.

Much thanks goes to my thesis advisor, Dr. Maybeck, for his patience, consideration, and above all expert advice given throughout this project. Dr. Kabrinsky deserves additional thanks for his assistance in the pattern recognition area. Finally, without the help of my experienced typist, Ms. Cheryl Nicol, this report would not have been completed.

James Singletery Jr.

Contents

	Page
Preface	ii
List of Figures	iv
List of Tables	vi
List of Symbols	vii
Abstract	ix
I. Introduction	1
Background	1
Problem Overview	3
Plan of Attack	7
II. Models and Data Processing Fundamentals	9
Karhunen-Loève Transformation	9
Fourier Transform	13
Averaging	19
Spatial Noise	20
Relationship Between Truth Model and Extended Kalman Filter	25
Truth Model	26
Extended Kalman Filter	31
Measurement Update	36
III. Performance Analysis	39
IV. Conclusions and Recommendations	50
Bibliography	52
Appendix A: Numerical Approximations	54
Appendix B: Coordinate System for 8 x 8 Input Array	57
Appendix C: Input Patterns	58
Appendix D: Computer Software	61
Vita	98

List of Figures

Figure		Page
1	Data Processing Scheme	5
2a	Finite Area A x B	16
2b	Sequence Numbers	16
3	FOURT Format	17
4	Rearranged Format	17
5	Pixel Numbering Scheme	21
6	First and Second Nearest Correlation Coefficients . . .	23
7	Results of Shift Routine	42
8	No Noise $\sigma = 1/4$ pixel $\alpha = 0.1$	43
9A	1st Run $\sigma = 1/4$ pixel S/N = 10 $\alpha = 0.1$	44
9B	50th Run $\sigma = 1/4$ pixel S/N = 10 $\alpha = 0.1$	44
10A	1st Run $\sigma = 1/4$ pixel S/N = 20 $\alpha = 0.1$	45
10B	50th Run $\sigma = 1/4$ pixel S/N = 20 $\alpha = 0.1$	45
11	No Noise IMAX = 20 $\sigma = 3$ pixels	46
12A	1st Run $\sigma = 3$ pixels S/N = 10 $\alpha = 0.1$	47
12B	50th Run $\sigma = 3$ pixels S/N = 10 $\alpha = 0.1$	47
13A	1st Run $\sigma = 3$ pixels S/N = 20 $\alpha = 0.1$	48
13B	50th Run $\sigma = 3$ pixels S/N = 20 $\alpha = 0.1$	48
14	Pixel Sampling Scheme	55
15	Coordinate System for Input Array	57
16a	40 x 40 Constant Intensity	59
16b	3 Constant Height Cylinders	59
16c	3 Gaussian Profiles	59
17a	Discrete 40 x 40 Constant Intensity	60

List of Figures

Figure		Page
17b	Discrete 3 Constant Height Cylinders	60
17c	Discrete 3 Gaussian Profiles	60

List of Tables

Table		Page
1	Divergence Analysis	49

List of Symbols

Symbol		Page
$\hat{\underline{x}}(t_i^+)$	state estimate after incorporation of measurement	3
$\hat{\underline{x}}(t_i^-)$	propagated state estimate vector before incorporation of measurement	3
$\underline{K}(t_i)$	Kalman Filter Gain	3
$\underline{z}(t_i)$	actual measurement vector	3
$h(\hat{\underline{x}}(t_i), t_i)$	non-linear h function	3
$R(x, \alpha; y, \beta)$	spatial autocorrelation kernel	9
$\phi_i(\alpha, \beta)$	eigenfunctions	9
λ_i	eigenvalues	9
$S(w_x, w_y)$	power density spectrum	11
$\Phi(jw_x, jw_y)$	Fourier Transform of $\phi_i(\alpha, \beta)$	11
T	Fourier Transform	12
f_x, f_y	spatial frequencies	13
x, y	spatial variables	13
m, n	sequence numbers in space domain	14
k, l	sequence numbers in spatial frequency domain	14
M, N	spatial area covered by the sequence numbers	14
$\hat{y}(t)$	most recent averaged value	19
y(t)	most recent piece of data	19
$\hat{y}(t-1)$	previous averaged value	19
α	exponential smoothing constant	19
\underline{C}	matrix of correlation coefficients	23
\underline{R}	correlation matrix	24

List of Symbols

Symbol		Page
$\underline{V}(t_i)$	measurement noise vector	24
$\underline{W}(t_i)$	white noise Gaussian vector	24
λ	correlation time	27
\underline{F}_T	truth model plant matrix	28
\underline{G}_T	truth model input matrix	28
$\Phi(t, t_i)$	state transition matrix	30
$P(t^+)$	conditional state covariance matrix from measurement update	34
$P(t_{i+1}^-)$	propagated conditional state covariance matrix .	34
\underline{Q}_F	noise covariance matrix	33
$\underline{H}(t_i)$	linear h function	36

10 to the -8th power

Abstract

Although a number of the major objectives that were established at the outset of this project were not met, a number of milestones were realized. The digital implementation of a negating phase shift that operates perfectly under ideal conditions was a major accomplishment. The establishment of a zero level of 10^{-8} was also significant. The incorporation of the exponential smoothing technique to minimize the effect of measurement noise was important since it uncovered a possible connection between the size of the target image and its performance throughout the pattern recognition process. However, the major obstacle that surface during the execution of this project was a filter divergence problem. It has been proposed that this problem can be solved by implementing the Fourier transform derivative property instead of the forward-backward difference method to compute the spatial derivative of the non-linear h function.

1 Introduction

Background

The application of laser technology to everyday life is growing in importance as each year passes. In areas from medicine to industry to military applications, laser technology, although in its embryonic stage, has gained a foothold and is destined to have a major impact on the future. For instance, in the industrial area, laser drilling has significantly improved the machining qualities resulting in smoother cuts, reduced tool force, and increased speed and accuracy (1:225-31). In the medical area, the application of lasers in ophthalmology is promising. For example, the use of lasers to repair retinal tears and holes has been quite successful (2:360-7). For military applications, the ability to deposit large amounts of laser energy onto targets is a major research effort. One in a number of major obstacles before realizing this application deals with the precision tracking of a target and the subsequent pointing of the laser beam. This thesis is one in a series of research efforts devoted to solving this problem.

Traditionally, correlation algorithms have been employed to provide pointing and tracking information to a system. This correlation tracker stores a set of predetermined or previous real-time data target images in memory, compares these images with the images from its sensors. In the process of performing the mathematical calculations to characterize the differences between the stored and actual images, the appropriate commands are sent to the tracker to minimize the offset between the two (3:30-8). However, two major disadvantages of the correlation algorithm are its susceptibility to noise and absence of sensitivity to target

dynamics (3:31). To combat these drawbacks, the use of an extended Kalman Filter algorithm in place of the correlation tracker is being explored.

The Kalman Filter is a computer algorithm which processes noise-corrupted measurements and provides a reasonably accurate estimate of the state variables of interest (4:3). The actual mathematical details of the Kalman Filter are contained in Chapter 2 under the subtitle Extended Kalman Filter.

As mentioned earlier, this project is one in a series of research efforts. To be more precise, this project is the follow-on to two other projects. The first of these, entitled "An Extended Kalman Filter For Use in a Shared Aperture Medium Range Tracker" by Daniel E. Mercier, dealt with a very benign distant point target which could be analytically expressed as a two-dimensional gaussian intensity profile of circular contours (3:6-7). This intensity profile and all other profiles developed for this research effort are assumed to be scanned by a Forward-Looking Infrared (FLIR) sensor. This sensor horizontally and vertically scans the system field of view (FOV) to provide an 8 x 8 array of discrete values. These discrete values represent the average intensity of that portion of the image which lay across the appropriate detector (3:4-5).

Using some of the results of Mercier's Thesis, the second project, entitled "An Adaptive Distributed Measurement Extended Kalman Filter For a Short Range Tracker" by Robert L. Jensen and Douglas A. Harnly, dealt with more dynamic targets at closer ranges but still assumed that the target intensity pattern could be expressed analytically. However, Jensen and Harnly's thesis did make provisions to adaptively change the

shape of unimodal intensity patterns (5:77). Still, for actual hardware implementation, a priori knowledge of the analytic form of the intensity often cannot be assumed. Instead, on-line numerical techniques will have to be exploited to provide the necessary information to the Kalman Filter. The development of these techniques and their subsequent interface with the Kalman Filter is the basis for this project.

Problem Overview

The numerical techniques mentioned toward the end of the previous section include the Fast Fourier Transform (FFT), the shift theorem of Fourier Transform, the exponential smoothing technique, and the forward-backward difference method. These techniques are discussed in more detail in Chapter 2 and Appendix A. However, all involve the manipulation of intensity measurements provided by the FLIR sensor. The end result of these computations is to provide information to the Kalman Filter about the intensity pattern shape. This information takes the form of certain components of the measurement update equation. A detailed description of the measurement update equation is contained in Chapter 2 under the subtitle Measurement Update. However, the general form of this equation is

$$\underline{\hat{x}}(t_i^+) = \underline{\hat{x}}(t_i^-) + \underline{K}(t_i) (\underline{z}(t_i) - \underline{h}(\underline{\hat{x}}(t_i^-)t_i)) \quad (1)$$

where $\underline{\hat{x}}(t_i^+)$ = state estimate vector after incorporation of measurement

$\underline{\hat{x}}(t_i^-)$ = propagated state estimate vector before incorporation of measurement

$\underline{K}(t_i)$ = Kalman Filter Gain

$\underline{z}(t_i)$ = actual measurement vector

$\underline{h}(\hat{\underline{x}}(t_1^-)t_1)$ = non-linear function of intensity measurement at time t_1 , as a function of the true state estimate

In devising this project, it was decided that under ideal conditions, the Kalman Filter would provide state estimates which would center the target images from one sample period to another. This desirability of producing centered images is motivated by the simplicity it produces in the Kalman Filter equations. If the center images correspond to state estimates equal to zero, the resulting measurement equations become

$$\hat{\underline{x}}(t_1^-) = \underline{0} \quad (2)$$

$$\hat{\underline{x}}(t_1^+) = \underline{0} + \underline{K}(t_1) (z(t_1) - h(0_1 t_1)) \quad (3)$$

where

$\underline{h}(0_1 t_1)$ = centered non-linear h function

The generation of $\underline{h}(0_1 t_1)$ involves the use of the FFT, shifting theorem, and exponential smoothing techniques mentioned earlier. The details of how these techniques are utilized will be discussed later however, buried within the Kalman Filter gain ($\underline{K}(t_1)$) is the spatial derivative of the centered non-linear h function (see Chapter 2, Equation 56). This spatial derivative is generated using the forward-backward difference method discussed in Appendix A.

The flow of the data processing scheme is shown in Figure 1. In essence, there are two parallel data processing paths for the intensity measurements. The first path involves taking the 8 x 8 array of intensity measurements and arranging it by rows into a 64 x 1 measurement vector. This vector is then provided, as a measurement $\underline{z}(t_1)$, to the extended Kalman Filter which in turn provides state estimates that are used in the second path to provide centered measurement functions. This

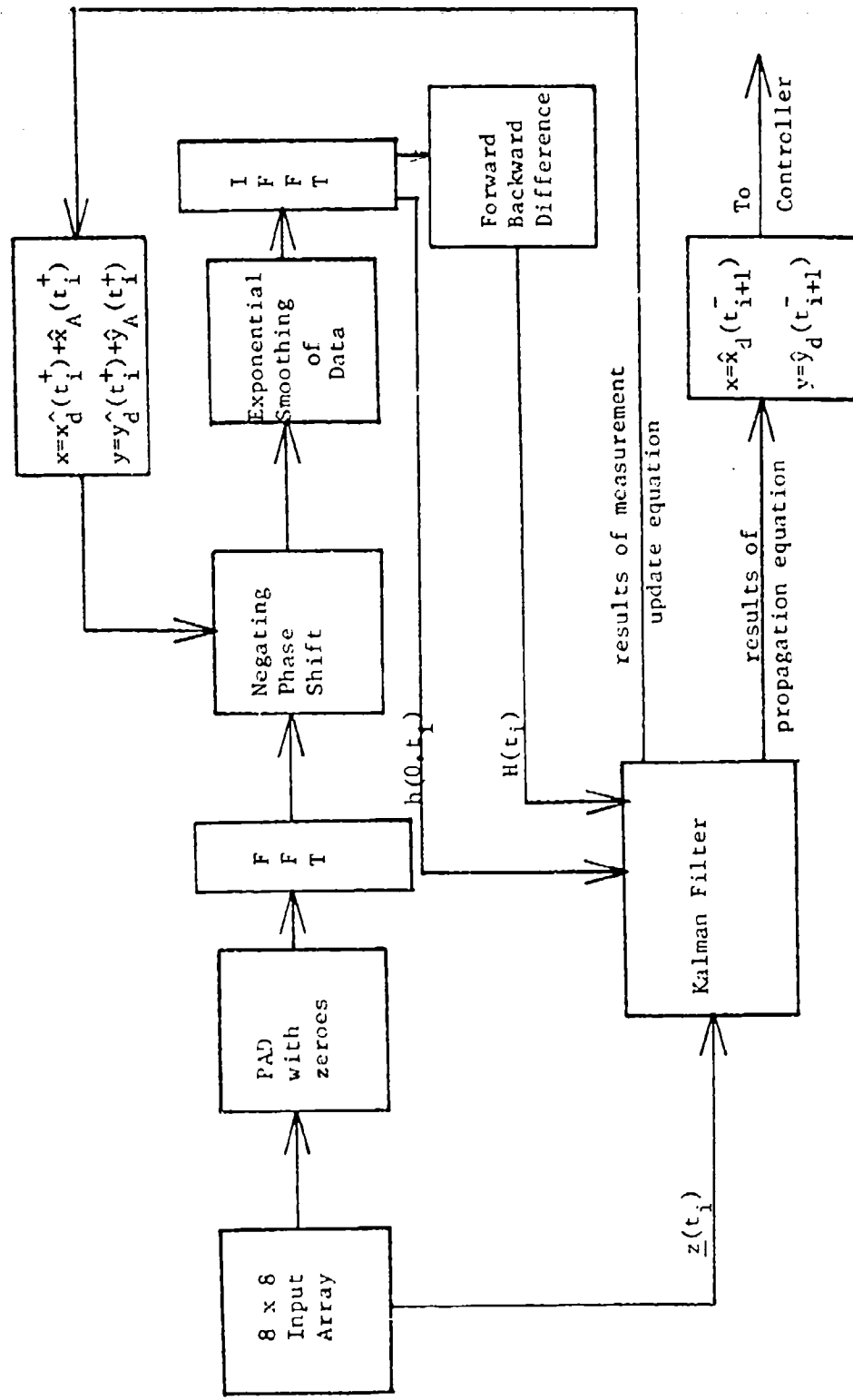


Figure 1. Data Processing Scheme

second path represents the main thrust of this thesis. Its purpose is to provide the centered non-linear and linear measurement functions mentioned earlier. To accomplish this, the shifting theorem of Fourier Transforms is exploited. In essence, the translation of an intensity pattern in the space domain can be negated by multiplying its Fourier Transform by the complex conjugate of the resulting linear phase shift (see Chapter 2, Fourier Transform). The source of the image translation about the FLIR array can be traced to two effects: the actual target dynamics and atmospheric jitter. An estimate of these effects are available from the Kalman Filter measurement update equations (see Chapter 2, Extended Kalman Filter). In turn, these best estimates are used in the argument of the complex conjugate of the linear phase shift to provide centered measurement functions. In addition, before the inverse Fourier Transform is taken, this centered pattern is averaged, using the exponential smoothing technique, with previous centered Fourier Transformed patterns to minimize the effect of measurement noise (see Chapter 2, Averaging). Once the inverse Fourier Transform is taken, the spatial derivative is then taken using the forward-backward difference approximation discussed in Appendix A to provide the centered linearized H function used in the calculation of the Kalman Filter Gain.

The sequential processing along the second path shown in Figure 1 together with its connection to the first path is an important fact. A copy of the 8 x 8 array of data is first padded with zeroes to alleviate problems in using the FFT (see Chapter 2, Fourier Transform). Next, the Fourier Transform of the two-dimensional array of data is taken. Before the negating phase shift is applied to this Fourier Transform, the processing of the measurement vector along the first path has to be

completed, since the resulting state estimates from the measurement update equation are used in the linear phase shift in the second data processing path. After applying the negating linear phase shift, this centered Fourier Transform is averaged with past centered Fourier Transforms to minimize the effect of noise. Next, the inverse Fourier Transform is taken which, theoretically, results in a centered pattern with noise effects substantially reduced. The zeroes that were initially added to the input array are stripped away with the remaining 8 x 8 data array representing the non-linear h function. In addition, using the numerical approximation discussed in Appendix A, the linearized H function is generated from this non-linear h function and both functions are used by the Kalman Filter for processing of the next measurement that becomes available.

An additional process that occurs along the first path is the propagation of the state estimate vector to the next sample time. This process provides the best prediction of where the target will be located just before the next measurement update is taken. Therefore, this information could be fed to a controller so as to minimize the perturbations of the image about the center of the FOV.

Plan of Attack

The plan of attack presented here provides a general flow of what will later be examined in greater detail in the performance analysis section. The verification of a pattern recognition algorithm along with its interface with the Extended Kalman Filter represents the basic premise upon which this thesis project was developed.

The verification of the pattern recognition algorithm is composed

of several different parts. These parts include verifying the FFT algorithm, verifying the ability to negate the translational effects in the space domain given perfect phase shift information to apply in the spatial frequency domain, and verifying the exponential smoothing technique as a means to minimize the effect of noise corruption on the measurement information.

The Extended Kalman Filter section involves measuring the impact of the non-linear and linearized h functions developed in the pattern recognition section on the performance of the Kalman Filter as compared to being given correct h functions. Also implicit in this verification is another comparison involving the use of state estimates from the Kalman Filter, instead of providing artificial knowledge of the true pattern offset, to provide the shift information needed in the pattern recognition section to provide centered patterns used to generate the h functions mentioned earlier (see Problem Overview).

II Models and Data Processing Fundamentals

Karhunen-Loève Transformation

In the area of pattern recognition, it is highly desirable to determine the optimal set of eigenfunctions and their corresponding eigenvalues to represent two-dimensional intensity patterns. This representation can be determined with the orthogonal Karhunen-Loève transformation

$$\int_{-y}^y \int_{-x}^x R(x,\alpha;y,\beta) \phi_i(\alpha,\beta) d\alpha d\beta = \lambda_i \phi_i(\alpha,\beta) \quad (4)$$

where $R(x,\alpha;y,\beta)$ = spatial autocorrelation kernel

$\phi_i(\alpha,\beta)$ = eigenfunctions

λ_i = eigenvalues

Based on properties specified through the spatial autocorrelation kernel, the entire information of an image is preserved by the given set of eigenvalues and eigenfunctions (6:6). Furthermore, since the low order terms normally provide the maximum sensitivity to target motion, the higher order terms of this spatial model decomposition can be neglected with little degradation in the quality of the resultant image (6:6).

As mentioned earlier, the key to finding the optimal set of functions is to know the spatial autocorrelation kernel. For intensity patterns represented by a two-dimensional discrete array of values, the correlation kernel is represented as a correlation matrix of dimension $N^2 \times N^2$ with N being the dimension of the square input matrix (6:6). The generation of this correlation matrix is a major drawback in using the Karhunen-Loève transformation. However, if this matrix can be assumed or determined, the transformation matrix (A) which diagonalizes

the correlation matrix (R) can be evaluated by:

$$A^T R A = \begin{bmatrix} \lambda_1 & & & \\ & \lambda_2 & & \\ & & \dots & \\ & & & \lambda_{N^2} \end{bmatrix} \quad (5)$$

where λ_1 's represents the eigenvalues in decreasing order of magnitude ($\lambda_1 \geq \lambda_2 \geq \dots \geq \lambda_{N^2}$) (6:6). Since the transformation matrix (A) is developed from orthogonal eigenvectors of the correlation matrix, the transformation matrix is orthogonal. Thus, the forward and reverse Karhunen-Loève transformations that will preserve the quality of the image are

$$\text{forward direction: } (F) = (f) (A)$$

$$\text{reverse direction: } (f) = (F) (A)^T$$

where (f) = image vector

(F) = resultant image vector in the transform domain

(A) = transformation matrix (6:7)

Once again, if the entire group of eigenvalues and eigenvectors were retained, the total quality of the image would be preserved. But, if only m of the first N^2 eigenvalues were retained, the resultant mean square error (MSE) between the reconstructed image and the initial image would be the sum of the eigenvalues not included in the transformation.

$$MSE = \sum_{i=m+1}^{N^2} \lambda_i \quad (6:7)$$

As discussed in the article "Image Processing by Computer" by Guy Hanuise, from which the Karhunen-Loève transformation argument has been developed, this transformation does possess some major disadvantages. The most significant drawbacks center around the generation of the correlation matrix. As the size of the square image matrix (N x N)

grows, the correlation matrix grows as N^2 (i.e. $N^2 \times N^2$). Thus, with large image quantization levels, serious data processing problems arise (6:7). Along the same lines, the exact calculation of the correlation matrix is very difficult to perform. As a result, more common orthogonal transformations such as the Fourier transform are used in signal processing. Implicit in the use of the Fourier transform are the assumptions of spatial stationarity of the autocorrelation kernel and a space domain infinite in extent. Referring back to equation 4, in applying the assumption of spatial stationarity, and a domain of infinite extent, the Karhunen-Loève transformation equation becomes

$$\int_{-\infty}^{\infty} \int_{-\infty}^{\infty} R(x-\alpha, y-\beta) \phi_i(\alpha, \beta) d\alpha d\beta = \lambda_i \phi_i(\alpha, \beta) \quad (6)$$

Upon close examination of equation 6, the integral equation would be recognized as a two-dimensional convolution of two functions (7:10). The unique feature of the convolution theorem that makes it very appealing is that in the other transform domain, the two functions are multiplied together. Therefore, the Fourier transform of equation 6 can be written as

$$S(w_x, w_y) \phi_i(jw_x, jw_y) = \lambda_i \phi_i(jw_x, w_y) \quad (7)$$

where $S(w_x, w_y) =$ Fourier transform of $R(x, y)$ (power density spectrum)

$$\phi_i(jw_x, jw_y) = \text{Fourier transform of } \phi_i(\alpha, \beta)$$

For the equality in equation 7 to hold either one of two conditions must be met: either $S(w_x, w_y) = \lambda_i$, which is an impossibility since the λ_i 's are scalar multiples and $S(w_x, w_y)$ is in a functional form, or more realistically, $\phi_i(jw_x, jw_y)$ is an impulse function. The choice of the impulse function would be appropriate since it can be set to sample the

power density spectrum at the particular value of w_x 's where the function equals the value of the scalar multiple.

$$\phi_i(jw_x, jw_y) = \delta(w_x - w_{xi}; w_y - w_{yi}) \quad (8)$$

Thus, by taking the inverse Fourier transform of this impulse function, the resulting eigenfunctions for the space domain are:

$$\phi_i(x, y) = T^{-1}(\delta(w_x - w_{xi}; w_y - w_{yi})) \quad (9)$$

$$* \phi_i(x, y) = \exp(j(w_{xi}x + w_{yi}y)) \quad (8:237-42) \quad (10)$$

In reality, the space domain is limited by the system FOV and the random process describing the image intensity may not be truly spatially stationary. However, if the system FOV is relatively large and the random process is quasi-stationary, it could be heuristically argued that the resulting eigenfunctions still asymptotically approach complex exponentials. This result would provide reasonable motivation to use complex exponentials (Fourier transform) as the transformation function on the images in question.

In closing this section, it should be reiterated that the Karhunen-Loève transformation is difficult to perform in its exact form. However, under the assumptions of spatial stationarity and a space domain large in extent, the Karhunen-Loève equation provides adequate motivation for using familiar transformations involving complex exponentials such as Fourier.

* This same argument has been developed for the one-dimensional case in Chapter 8 of Introduction to Statistical Pattern Recognition by Keinosuke Fukunaga.

Fourier Transform

The Fourier transform is a familiar transformation to the electrical engineer. In the one dimensional case, it is a transform quite often used to relate occurrences in the time domain to those in the frequency domain. However, with the ability of lenses to perform Fourier transforming instantaneously, the field of Fourier optics has provided motivation for extending the concept of the Fourier transform and its properties into two-dimensional space. As a result of this extension, the two-dimensional Fourier transform becomes

$$G(f_x, f_y) = \int_{-\infty}^{\infty} \int_{-\infty}^{\infty} g(x, y) \exp -j2\pi(f_x x + f_y y) dx dy \quad (7:5) \quad (11)$$

where

$G(f_x, f_y)$ = Fourier or Frequency Spectrum

$g(x, y)$ = Function in the Space Domain

f_x, f_y = Spatial Frequencies

x, y = Spatial Variables

In comparing the one-dimensional and two-dimensional Fourier transforms, similarities should be recognizable; the use of the complex exponential as the eigenfunction, and the generation of spatial frequencies f_x, f_y to correspond with the spatial coordinate x and y . A particular property that has been extended to the two-dimensional case which is a vital part of this thesis is the shift theorem. The shift theorem states that a translation of an image in the space domain results in a linear phase shift in the spatial frequency domain:

$$\mathcal{T}\{g(x-a, y-b)\} = G(f_x, f_y) \exp(-j2\pi(f_x a + f_y b)) \quad (7:9) \quad (12)$$

where

a = offset of the spatial function along the x direction from a centered position

b = offset of the spatial function along the y direction from a centered position

To negate the translational effects in the space domain, the Fourier transform of the translated image is multiplied by the complex conjugate of the linear phase shift:

$$g(x,y) = T^{-1}\{G(f_x, f_y) \exp(-j2\pi(f_x a + f_y b)) \exp(j2\pi(f_x a + f_y b))\} \quad (13)$$

Up to now, the continuous case of the Fourier transform has been discussed, but to utilize the Fourier transform and its properties for computer simulation, the discrete form of the Fourier equations must be used. Such a development is contained in Digital Signal Processing by Alan V. Oppenheim and Ronald W. Schaffer. The discrete Fourier transform and the discrete version of the shift theorem are as follows:

$$T(x(m,n)) = \frac{1}{MN} \sum_{k=0}^{M-1} \sum_{\ell=0}^{N-1} \chi(k,\ell) \exp\left(-\frac{j2\pi k m}{M}\right) \exp\left(-\frac{j2\pi \ell n}{N}\right) \quad (14)$$

Discrete Fourier Transform (9:115)

$$T(x(m-m_0, n-n_0)) = \frac{1}{MN} \sum_{k=0}^{M-1} \sum_{\ell=0}^{N-1} \chi(k,\ell) \exp\left(-\frac{j2\pi k m}{M}\right) \exp\left(-\frac{j2\pi \ell n}{N}\right) \\ \times \exp\left(-\frac{j2\pi k m_0}{M}\right) \exp\left(-\frac{j2\pi \ell n_0}{N}\right) \quad (15)$$

$$0 \leq m_0 \leq M \quad 0 \leq n_0 \leq N$$

Discrete Shift Theorem (9:110)

where m,n = sequence numbers in the space domain

k,ℓ = sequence numbers in spatial frequency domain

M,N = spatial area covered by the sequence numbers

m_0, n_0 = translation of discrete pattern about its centered location.

As the definition of the variables may imply, the use of the discrete Fourier transform implies certain knowledge is known. In essence, the discrete Fourier transform views a finite area as being repeated indefinitely in both the x and y directions. Therefore, the establishment of the two-dimensional periodicity is imperative. The discretization of the finite area is reflected in the sequence numbers. The relationship between the sequence numbers and distance in the original space domain is shown in Figure 2. Notice that each pair of sequence numbers represent a smaller area within the previously mentioned finite area. For application to this thesis, the smaller area is represented by 20 urad x 20 urad with the total finite area being 480 urad x 480 urad. This results in the sequence numbers (m,n) varying from 1 to 24. Thus the sequence lengths (M,N) equal 24.

In the computer software for this project, a more efficient version of the discrete Fourier transform known as the Fast Fourier Transform (FFT) is used. The FFT and the Inverse Fast Fourier Transform (IFFT) are performed using a subroutine called FOURT. FOURT is a multi-dimensional FFT routine which uses the Cooley-Tukey method of calculation (10:76-9). A unique feature of the FOURT subroutine is the arrangement of the data array in the spatial frequency domain. As a result of the FOURT software, the FOURT format locates the D.C. term (zero frequency) in the upper left hand corner and the harmonics are misaligned as shown in Figure 3. In order to perform signal processing in the spatial frequency domain, the data array quadrants are switched, 2 with 4 and 1 with 3 (11:17). As shown in Figure 4, for an M by N dimension array, where M

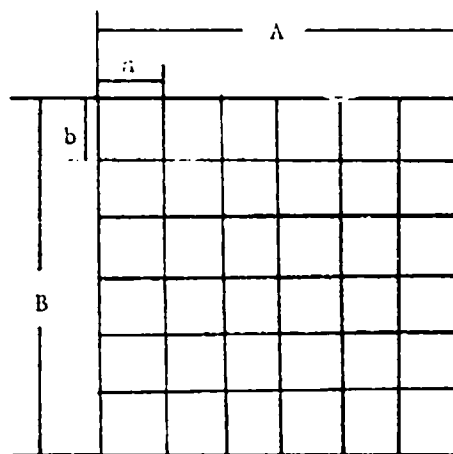


Figure 2A. Finite Area A x B

$(1,1)$	$(1,2)$	$(1,3)$	$(1,4)$	$(1,5)$	$(1,6)$
$(2,1)$	$(2,2)$	$(2,3)$	$(2,4)$	$(2,5)$	$(2,6)$
$(3,1)$	$(3,2)$	$(3,3)$	$(3,4)$	$(3,5)$	$(3,6)$
$(4,1)$	$(4,2)$	$(4,3)$	$(4,4)$	$(4,5)$	$(4,6)$
$(5,1)$	$(5,2)$	$(5,3)$	$(5,4)$	$(5,5)$	$(5,6)$
$(6,1)$	$(6,2)$	$(6,3)$	$(6,4)$	$(6,5)$	$(6,6)$

Figure 2B. Sequence Numbers

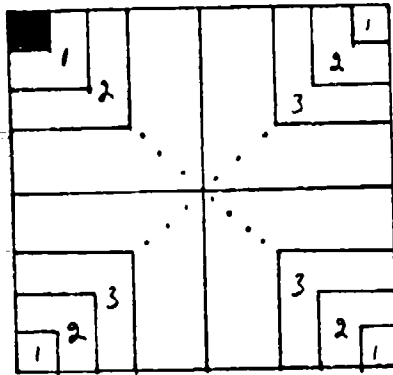


Figure 3. FOURT Format

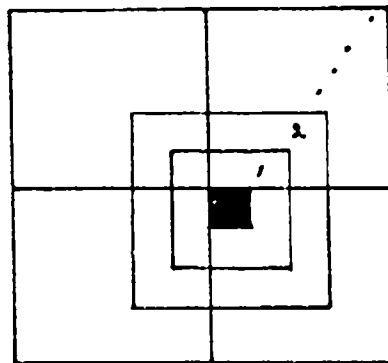


Figure 4. Rearranged Format

and N have to be even numbers, this rearranged format results in the D.C. term located at $(\frac{M}{2} + 1, \frac{N}{2} + 1)$ with the first concentric window surrounding the D.C. term being the first harmonic and corresponding higher harmonics matching with its appropriate window (11:18). Once the signal processing has taken place, the data array has to be rearranged back into the FOURT format before the IFFT is taken (11:19-21).

Another requirement for FFT processing is to pad the input data array with zeroes to reduce edge effects, aliasing, and leakage conditions. A precise definition of all three of these conditions as they apply to FFT's is difficult to come by. However, the effect of these three conditions is related to how the FFT views the finite area as one period in a domain infinite in extent. For a finite area unpadded with zeroes, there is a chance that important information clustered along the edges can be viewed as part of the adjacent period thus causing distortion in the FFT and subsequent image from the IFFT (11:13, 92-3). To prevent this possible distortion from occurring with this project, the original 8 x 8 array of FLIR data is arbitrarily padded with an additional 8 rows of zeroes on the top, bottom, and sides. This additional padding results in the 24 x 24 input array mentioned earlier in this section.

In summary, the FFT and IFFT processes for this project is done using the FOURT subroutine. To negate the translational effects on an image, the shift theorem of the Fourier transform will be digitally implemented. Finally, to eliminate possible distortion by edge effects, aliasing and leakage conditions, the original 8 x 8 array of data is padded with additional zeroes.

Averaging

In reality, the existence of a noise-free environment is fictitious. For computer simulations, this noise could be added to a computer-generated noise-free image. The actual details of how the noise corruption simulation is accomplished is discussed in the next section. Nonetheless, the noise effects can be minimized by appropriate data processing techniques. Since a priori knowledge of the precise form of the noise is normally not available, the underlying mathematics makes little assumption about the precise form. However, it is necessary to assume that the noise changes faster from sample period to sample period than the image pattern itself. Traditionally, the moving average technique is used to combat the effect of noise under these conditions. This technique would store the most recent $K-1$ pieces of data in memory and average the data in memory with the new data in memory with the new piece of data using a weighting factor of $1/K$ on each piece of data (12:115). However, this technique does have one major disadvantage. It would require K storage locations of computer memory for each pixel. Therefore, for an $N \times N$ input array, KN^2 storage locations of computer memory is required. Thus, for large K and large input arrays, significant data processing problems would arise. An alternative method which alleviates this problem associated with the moving average is called exponential smoothing (12:114-28). The equation that is fundamental to this process is:

$$\hat{y}(t) = \alpha y(t) + (1-\alpha) \hat{y}(t-1) \quad (12:115) \quad (16)$$

where $\hat{y}(t)$ = most recent averaged value

$y(t)$ = most recent piece of data

$\hat{y}(t-1)$ = previous averaged value

α = smoothing constant

$$0 \leq \alpha \leq 1$$

A key parameter in the exponential smoothing equation is the smoothing constant α which can vary anywhere from 0 to 1 inclusive, depending on how much $\hat{y}(t)$ is to respond to the most recent piece of data. For noisy data and slowly changing signal pattern, it is suggested that the values of α tend more toward 0 than 1 so that there is some damping of the noise, yet there is still some response to the most recent piece of data (12: 115). For this thesis project, a steady state value of 0.1 for the smoothing constant was assumed. The notion of steady state value is important since a pseudo-exponential smoothing technique is used to provide better sensitivity to the initial 10 pieces of data. In essence, the smoothing constant is varied for each of the first ten runs (i.e. $\alpha = 1/K$ $K = 1, 2, 3, \dots, 10$) until the steady state value of $\alpha = 0.1$ was reached.

In closing this section, it is interesting to note that the exponential smoothing technique possesses those qualities that the moving average lack. First, only $2N^2$ computer storage locations are needed to generate $\hat{y}(t)$. Second, $\hat{y}(t)$ contains portions of all past $\hat{y}(t)$'s although the initial pieces of data have less of an impact on the most recent averaged value.

Spatial Noise

To model the real world environment, noise corruption should be added to any computer simulation. There are two general types of characteristics to specify for the noise corruption in this problem, temporal and spatial. Temporally correlated noise implies that knowing

something about the noise at one particular time infers something about the noise at a later time. Normally, this inference can be modelled by a correlation function that is exponential in shape (5:37). However, since temporally correlated noise corruption has little effect on the quality of the image beyond that of temporally uncorrelated noise at the expected signal-to-noise ratio for this application, and since it is difficult to implement in a computer simulation, it was not included in this thesis project (5:37).

Under spatial noise characteristics, there are two categories, spatially uncorrelated and correlated noise. Before examining these two areas, a number system for the 8 x 8 input pixel array and the 64 x 64 resultant correlation matrix have to be developed. The 8 x 8 array is numbered from 1 to 64 by rows starting in the upper left-hand corner (Figure 5).

1	2	3	4	5	6	7	8
9	10	11	12	13	14	15	16
17	18	19	20	21	22	23	24
25	26	27	28	29	30	31	32
33	34	35	36	37	38	39	40
41	42	43	44	45	46	47	48
49	50	51	52	53	54	55	56
57	58	59	60	61	62	63	64

Figure 5. Pixel Numbering Scheme (5:19)

In the associated 64 x 64 correlation matrix, each row or column represents how that particular pixel relates to the other pixels in the input array. For example, row 1 or column 1 represents the correlation for how pixel 1 relates to itself and the other 63 pixels. Two unique

features of the correlation matrix are (1) since the correlation between two pixels is the same in both directions (i.e. $r_{ij} = r_{ji}$), the correlation matrix is symmetric and (2) since the correlation coefficient is one for a pixel related to itself, the diagonal elements of the matrix are one. In determining the off diagonal terms, the first and second nearest neighbor concept discussed in Harnly and Jensen's thesis was used (5:18-20). Essentially, the exponential form of the correlation function is assumed in generating the correlation coefficients. However, the non zero values generated are limited to the first and second nearest neighbors of the pixel in question. This condition results in 25 out of 64 entries in each row or column being nonzero. Of these 25 values, there are only six distinct values; one for the correlation coefficient of the pixel with itself, four values of 0.3679, four values of 0.2431, four values of 0.1353, eight values of 0.1069, and four values of 0.0591. These nonzero values, which are used to generate the 64 x 64 correlation coefficient matrix (C), were developed from the following equation

$$C_{ij} = \exp\left(-\frac{d_{ij}}{20}\right) \quad (17)$$

where d_{ij} = distance from center of pixel i to center of pixel j

The choice of a correlation distance of 20 urad is dictated by the non-zero values generated by the first and second nearest neighbor concept (Figure 6).

$C_5 = 0.0591$	$C_4 = 0.1069$	$C_3 = 0.1353$	$C_4 = 0.1609$	$C_5 = 0.0591$
$C_4 = 0.1069$	$C_2 = 0.2431$	$C_1 = 0.3679$	$C_2 = 0.2431$	$C_4 = 0.1609$
$C_3 = 0.1353$	$C_1 = 0.3679$	$C_0 = 1$	$C_1 = 0.3679$	$C_3 = 0.1353$
$C_4 = 0.1069$	$C_2 = 0.2431$	$C_1 = 0.3679$	$C_2 = 0.2431$	$C_4 = 0.1609$
$C_5 = 0.0591$	$C_4 = 0.1069$	$C_3 = 0.1353$	$C_4 = 0.1609$	$C_5 = 0.0591$

Figure 6. First and Second Nearest Correlations Coefficient

For the spatially correlated case, the matrix of correlation coefficients becomes

$$\underline{C} = \begin{bmatrix} 1 & C_{1,2} & C_{1,3} & \dots & C_{1,64} \\ C_{1,2} & 1 & C_{2,3} & \dots & C_{2,64} \\ C_{1,3} & C_{2,3} & 1 & \dots & C_{3,64} \\ \dots & \dots & \dots & \dots & \dots \\ C_{1,64} & C_{2,64} & C_{3,64} & \dots & 1 \end{bmatrix}$$

To complete the process for generating the noise, the 64 x 64 correlation

coefficient matrix is pre-multiplied by the scalar value of the variance σ_n^2 in order to generate the correlation matrix itself.

$$\underline{R} = \sigma_n^2 \underline{C} = \sigma_n^2 \begin{bmatrix} 1 & C_{1,2} & C_{1,3} & \dots & C_{1,64} \\ C_{1,2} & 1 & C_{2,3} & \dots & C_{2,64} \\ C_{1,3} & C_{2,3} & 1 & \dots & C_{3,64} \\ \dots & \dots & \dots & \dots & \dots \\ C_{1,64} & C_{2,64} & C_{3,64} & \dots & 1 \end{bmatrix}$$

Now that \underline{R} is known, the 64 x 1 noise vector ($\underline{V}(t_i)$), which will be added to the input array, can be computed by using the Cholesky square root. Specifically,

$$\underline{V}(t_i) = \underline{\mathcal{C}}\underline{R} \underline{W}(t_i) \quad (18)$$

where $\underline{W}(t_i) = 64$ - dimensional independent white Gaussian noise vector (zero mean, variance of \underline{I})

$$\text{thus } E(\underline{W}(t_i) \underline{W}^T(t_j)) = \underline{I} \delta_{ij}$$

The Cholesky square root is a unique matrix decomposition which produces the square root of \underline{R} in the lower triangular form. This lower triangular form minimizes the number of nonzero computations in generating $\underline{V}(t_i)$.

To recover the original \underline{R} matrix, the $\underline{\mathcal{C}}\underline{R}$ should be post-multiplied by $\underline{\mathcal{C}}\underline{R}^T$ therefore $\underline{\mathcal{C}}\underline{R} \underline{\mathcal{C}}\underline{R}^T = \underline{R}$. Because of this property, the covariance of $\underline{V}(t_i)$ is preserved with the use of the Cholesky square root:

$$\begin{aligned} E(\underline{V}(t_i) \underline{V}^T(t_j)) &= E(\underline{\mathcal{C}}\underline{R} \underline{W}(t_i) \underline{W}^T(t_j) \underline{\mathcal{C}}\underline{R}^T) \\ &= \underline{\mathcal{C}}\underline{R} E(\underline{W}(t_i) \underline{W}^T(t_j)) \underline{\mathcal{C}}\underline{R}^T = \underline{\mathcal{C}}\underline{R} \underline{I} \underline{\mathcal{C}}\underline{R}^T \delta_{ij} \\ &= \underline{R} \delta_{ij} \end{aligned} \quad (19)$$

As mentioned earlier, the noise vector will be added to the noise-free input matrix to model real-world image conditions. This resulting vector called $\underline{z}(t_i)$ is the measurement vector that will be provided to the Extended Kalman Filter. Algebraically, the z vector is developed from the truth model and is of the form

$$\underline{z}(t_i) = \underline{h}(\underline{x}(t_i), t_i) + \underline{v}(t_i) \quad (20)$$

where $\underline{x}(t_i)$ = output state vector from the system dynamics model

$\underline{h}(\underline{x}(t_i), t_i)$ = nonlinear measurement function developed from image intensity pattern

$\underline{v}(t_i)$ = measurement noise vector

As discussed in the problem overview, the development of the nonlinear h function from the measurement vector $\underline{z}(t_i)$ is a major goal of this thesis.

In summary, since temporally correlated noise has been shown to have little effect on the Kalman Filter performance at the signal-to-noise ratios for this project, only spatially correlated and uncorrelated noise was used. The correlation matrix used to generate the noise vector $\underline{v}(t_i)$ is developed from the first and second nearest neighbor concept as it applies to a correlation function exponential in nature. The Cholesky square root of the correlation matrix is taken and post-multiplied by a white noise vector $\underline{w}(t_i)$, with the final result being the noise vector $\underline{v}(t_i)$ that is added to the noise-free image array to provide the necessary noise corruption.

Relationship Between Truth Model and Extended Kalman Filter

In the previous section, terms such as truth model, system dynamics, and Extended Kalman Filter were used. These terms represent the heart

of this project. The truth model is a best representation of the environment from which the measurement vector $\underline{z}(t_i)$ is generated. These environmental characteristics include the underlying target dynamics, atmospheric effects, and background noise. In order to process the measurement vector $\underline{z}(t_i)$ and provide a best estimate of the underlying target centroid location for the next sample period, the Extended Kalman Filter is used. The actual details of the filter will be discussed in a later section. However, the interplay between the Kalman Filter and the truth model is a point which at times can be confusing. In order to provide a best estimate of the underlying centroid location, the dynamic models are a facsimile of those in the truth model. Ideally, the models should match exactly, but in reality, due to the desire for computational efficiency, there are always deviations. The amount of deviation in the dynamics models for the filter varies depending on the problem application. A contributing factor to this deviation may be a lack of knowledge concerning the exact form of the truth models. However, due to the robustness of the Kalman filter, adequate predictions of the centroid location can still be accomplished.

Truth Model

Much has been discussed concerning the dynamic models. For this project, it had been envisioned to investigate the feasibility of using both deterministic and stochastic models. In the realm of deterministic models, initially, the target dynamics involved a stationary target centered in the system FOV. This step was taken to identify and eliminate any possible inherent motion caused by the pattern recognition or Extended Kalman Filter algorithms. The next deterministic model involved

a target moving across the image plane at a constant velocity. This was done to test the robustness of the Extended Kalman Filter. Supposedly, the filter design used for this project can absorb any truth model whose resultant motion from one sample period to the next is less than one-half pixel (i.e. less than 10 urads) (13).

In the realm of stochastic models, the target and atmospheric dynamics developed in Mercier's thesis were used (3:9-16). The target dynamics are modelled in each direction as a first-order Gauss-Markov process driven by white Gaussian noise

$$\dot{X}_D(t) = -\frac{1}{\lambda_T} X_D(t) + W_1(t) \quad (16)$$

$$\dot{Y}_D(t) = -\frac{1}{\lambda_T} Y_D(t) + W_2(t) \quad (17)$$

$$\text{where } E(W_1(t)) = E(W_2(t)) = 0 \quad (18)$$

$$E(W_1(t) W_2(s)) = E(W_2(t) W_1(s)) = \frac{2\sigma_d^2}{\lambda_T} \delta(t-s) \quad (19)$$

$$E(W_1(t) W_2(s)) = 0 \quad (20)$$

λ_T = truth model correlation time

$W_1(t), W_2(t)$ = continuous time independent white Gaussian noise processes

σ_d^2 = the desired variance on the outputs X_D and Y_D (3:10).

The atmospheric jitter model was based on a study by the Analytic Sciences Corporation (14:29,30) and a data analysis by Hogge and Butts (15). These studies resulted in the development of a third order shaping filter, with a single pole at 14.14 rad/sec and a double pole at 659.5 rad/sec, that is driven by white Gaussian noise (3:12).

Since any n^{th} order differential equation can be written as a set

of coupled first order differential equations, the state space model incorporating both the target dynamics and atmospheric effects was generated using the Jordan canonical form (3:13). Referring to the state space model from Mercier's thesis,

$$\dot{\underline{X}}_T = \underline{F}_T \underline{X}_T + \underline{G}_T \underline{W}_T(t) \quad (21)$$

where \underline{F}_T = the truth model plant matrix

\underline{X}_T = the truth model state vector

\underline{G}_T = the truth model input matrix

\underline{W}_T = a vector of white Gaussian noise inputs

$$E\{\underline{W}_T(t)\} = 0 \quad (22)$$

$$E\{\underline{W}_T(t) \underline{W}_T^T(s)\} = \underline{Q}_T \delta(t-s) \quad (23)$$

$$\underline{Q}_T = \begin{bmatrix} \frac{2\sigma_d^2}{\lambda_T} & 0 & 0 & 0 \\ 0 & 1 & 0 & 0 \\ 0 & 0 & \frac{2\sigma_d^2}{\lambda_T} & 0 \\ 0 & 0 & 0 & 1 \end{bmatrix} \quad (24)$$

$$\underline{F}_T = \begin{bmatrix} -\frac{1}{\lambda_T} & 0 & 0 & 0 & 0 & 0 & 0 & 0 \\ 0 & -a & 0 & 0 & 0 & 0 & 0 & 0 \\ 0 & 0 & -b & 1 & 0 & 0 & 0 & 0 \\ 0 & 0 & 0 & -b & 0 & 0 & 0 & 0 \\ 0 & 0 & 0 & 0 & -\frac{1}{\lambda_T} & 0 & 0 & 0 \\ 0 & 0 & 0 & 0 & 0 & -a & 0 & 0 \\ 0 & 0 & 0 & 0 & 0 & 0 & -b & 1 \\ 0 & 0 & 0 & 0 & 0 & 0 & 0 & -b \end{bmatrix} \quad (25)$$

$$a = 14.14 \text{ rad/sec} \quad b = 659.5 \text{ rad/sec}$$

$$\underline{G}_T = \begin{bmatrix} 1 & 0 & 0 & 0 \\ 0 & G_1 & 0 & 0 \\ 0 & G_2 & 0 & 0 \\ 0 & G_3 & 0 & 0 \\ 0 & 0 & 1 & 0 \\ 0 & 0 & 0 & G_1 \\ 0 & 0 & 0 & G_2 \\ 0 & 0 & 0 & G_3 \end{bmatrix} \quad (26)$$

$$G_1 = \frac{ab^2}{(a-b)^2} \quad G_2 = -G_1 \quad G_3 = \frac{ab^2}{(a-b)} \quad (3:11-14)$$

The composition of these truth model matrices is dictated by the components of the truth model state vector describing the target dynamics and atmospheric effect on the centroid location. For this project from \underline{x}_T ,

$$\underline{x}_D = \underline{x}(1) \quad (27)$$

$$X_A + X(2) + X(3) \quad (28)$$

$$Y_D = X(5) \quad (29)$$

$$Y_A = X(6) + X(7) \quad (3:14) \quad (30)$$

where X_A and Y_A are atmospheric jitter variables as output of third order shaping filter.

In order to transition the state vector from one sample period to another, propagation equations are developed. The basis for these equations is the solution to the matrix differential equation

$$\dot{\underline{\Phi}}(t, t_i) = \underline{F}_T \underline{\Phi}(t, t_i) \quad (31)$$

where $\underline{\Phi}(t, t_i)$ = state transition matrix from time t_i to time t
associated with the matrix \underline{F}_T

$$\underline{\Phi}(t_i, t_i) = \underline{I} \quad (3:14) \quad (32)$$

Since the truth model plant matrix \underline{F}_T is a constant, the state transition matrix is stationary with respect to time. Therefore, $\underline{\Phi}(t_{i+1}, t_i)$ is also constant for a fixed sample period (3:14). Using this truth model plant matrix, the solution to the above differential equation becomes

$$\underline{\Phi}_T(\Delta t) = \begin{bmatrix} e^{-\Delta t/\lambda T} & 0 & 0 & 0 \\ 0 & e^{-a\Delta t} & 0 & 0 \\ 0 & 0 & e^{-b\Delta t} & te^{-b\Delta t} \\ 0 & 0 & 0 & e^{-b\Delta t} \end{bmatrix} \quad (33)$$

$$\Delta t = (t_{i+1} - t_i)$$

The state transition matrix is used in the solution to the state space vector differential equation

$$\dot{\underline{X}}_T = \underline{F}_T \underline{X}_T(t) + \underline{G}_T \underline{W}_T(t) \quad (34)$$

This solution is

$$\underline{X}_T(t_{i+1}) = \underline{\Phi}_T(\Delta t) \underline{X}_T(t_i) \quad (35)$$

$$+ \int_{t_i}^{t_{i+1}} \underline{\Phi}_T(t_{i+1}, \lambda) \underline{G}_T(\lambda) \underline{W}_T(\lambda) d\lambda \quad (36)$$

The details for the following argument are contained in Mercier's thesis. Nonetheless, the resulting equivalent discrete-time model to the above equation is

$$\underline{X}_T(t_{i+1}) = \underline{\Phi}_T(\Delta t) \underline{X}_T(t_i) + \sqrt{\underline{Q}_d} \underline{W}_d(t_i) \quad (37)$$

where $\sqrt{\underline{Q}_d}$ is the Cholesky square root of

$$\underline{Q}_d = \int_{t_i}^{t_{i+1}} \underline{\Phi}_T(t_{i+1}, \lambda) \underline{G}_T(\lambda) \underline{Q}_T(\lambda) \underline{G}_T^T(\lambda) \underline{\Phi}_T^T(t_{i+1}, \lambda) d\lambda \quad (38)$$

$$E\{\underline{W}_d(t_i)\} = \underline{0} \quad (39)$$

$$E\{\underline{W}_d(t_i) \underline{W}_d^T(t_i)\} = \underline{I} \lambda_{ij} \quad (3:14-5) \quad (40)$$

In summary, three truth models were developed for this project. Two models were deterministic in nature; a stationary target and a target moving at a constant velocity across the image plane. These models were primarily developed to trouble-shoot and provide a bench mark for the pattern recognition and Extended Kalman Filter algorithms. The third model is the stochastic representation that will ultimately be used to analyze the Filter performance.

Extended Kalman Filter

As stated before, the basic Extended Kalman Filter developed in Mercier's thesis was used for this project. The target dynamics assumed

by the Filter is also a first order Gauss-Markov process, generated by a first-order lag driven by white Gaussian noise (3:19). The differential equation describing a particular state, which is very similar to that for the stochastic truth model, is

$$\dot{X}(t) = -\frac{1}{\lambda} X(t) + W(t) \quad (41)$$

$$E(W(t)) = 0 \quad (42)$$

$$E(W(t) W(s)) = \frac{2\sigma^2}{\lambda} \delta(t-s) \quad (43)$$

where λ = correlation time

$X(t)$ = state

$\dot{X}(t)$ = time derivative of the state

$W(t)$ = white Gaussian noise (3:19)

However, the plant, input, and white noise covariance matrices assumed by the filter differ from those developed in the truth model. The reduced order filter design assumes four states in its state vector $(X_D, Y_D, X_A, Y_D)^T$ which results in a state vector differential equation

$$\dot{\underline{X}}_F(t) = \underline{F}_F \underline{X}_F(t) + \underline{W}_F(t) \quad (44)$$

where $\underline{X}_F(t)$ = filter state vector

\underline{F}_F = filter plant matrix

$\underline{W}_F(t)$ = input white noise vector

$$\underline{F}_F = \begin{bmatrix} -\frac{1}{\lambda_D} & 0 & 0 & 0 \\ 0 & -\frac{1}{\lambda_D} & 0 & 0 \\ 0 & 0 & -\frac{1}{\lambda_A} & 0 \\ 0 & 0 & 0 & -\frac{1}{\lambda_A} \end{bmatrix} \quad (45)$$

λ_D = correlation time assumed for target dynamics

λ_A = correlation time assumed for atmospheric jitter

$$E(\underline{w}_F(t)) = 0 \quad (46)$$

$$E(\underline{w}_F(t) \underline{w}_F^T(s)) = \underline{Q}_F \delta(t-s) \quad (47)$$

$$\underline{Q}_F = \begin{bmatrix} \frac{2\sigma_D^2}{\lambda_D} & 0 & 0 & 0 \\ 0 & \frac{2\sigma_D^2}{\lambda_D} & 0 & 0 \\ 0 & 0 & \frac{2\sigma_A^2}{\lambda_A} & 0 \\ 0 & 0 & 0 & \frac{2\sigma_A^2}{\lambda_A} \end{bmatrix} \quad (48)$$

σ_D^2 = assumed target dynamics noise variance

σ_A^2 = assumed atmospheric noise variance (3:20)

It should be mentioned that the values of the \underline{Q}_F matrix are determined during the off-line tuning process designed to produce the optimal tracking performance (16:224).

As with the truth model, the Kalman Filter performs a propagation of its state estimate vector and conditional covariance matrix from one sample time to the next. The state transition matrix is also developed from a differential equation similar to that used in the truth model, except the filter plant matrix is used instead of the truth model plant matrix.

$$\dot{\underline{\Phi}}_F(t, t_i) = \underline{F}_F \underline{\Phi}_F(t, t_i) \quad (3:21) \quad (49)$$

$$\underline{\Phi}(t_i, t_i) = \underline{1} \quad (50)$$

Since \underline{F}_F is a time invariant matrix, the solution to the above differential equation is $\underline{\Phi}_F(t, t_i)$, the filter state transition matrix, given by

$$\underline{\Phi}_F(t, t_i) = \begin{bmatrix} e^{-(t-t_i)/\lambda_D} & 0 & 0 & 0 \\ 0 & e^{-(t-t_i)/\lambda_D} & 0 & 0 \\ 0 & 0 & e^{-(t-t_i)/\lambda_A} & 0 \\ 0 & 0 & 0 & e^{-(t-t_i)/\lambda_A} \end{bmatrix} \quad (51)$$

In solving the associated differential equation for the propagation of the covariance matrix, the following stochastic integral equation results:

$$\begin{aligned} \underline{P}(t_{i+1}^-) &= \underline{\Phi}_F(t_{i+1}, t_i) \underline{P}(t_i^+) \underline{\Phi}_F^T(t_{i+1}, t_i) \\ &+ \int_{t_i}^{t_{i+1}} \underline{\Phi}_F(t_{i+1}, \lambda) \underline{Q}_F(\lambda) \underline{\Phi}_F^T(t_{i+1}, \lambda) d\lambda \end{aligned} \quad (52)$$

where $\underline{\Phi}_F(t_{i+1}, t_i)$ = filter state transition matrix

$\underline{P}(t_i^+)$ = conditional state covariance matrix from measurement update equation at time t_i

$\underline{P}(t_{i+1}^-)$ = conditional state covariance matrix propagated from time t_i to t_{i+1}

$\underline{Q}_F(\lambda)$ = noise covariance matrix (3:21)

Using the \underline{Q}_F matrix specified in equation 48, the solution to the integral term in the stochastic equation above becomes

$$\begin{bmatrix}
 \sigma_D^2(1-e(-\frac{2\Delta t}{\lambda_D})) & 0 & 0 & 0 \\
 0 & \sigma_D^2(1-e(-\frac{2\Delta t}{\lambda_D})) & 0 & 0 \\
 0 & 0 & \sigma_A^2(1-e(-\frac{2\Delta t}{\lambda_A})) & 0 \\
 0 & 0 & 0 & \sigma_A^2(1-e(-\frac{2\Delta t}{\lambda_A}))
 \end{bmatrix} \quad (53)$$

To solidify the development of the propagation equations, the following summary of the estimated state vector and the conditional covariance matrix propagation equations is presented.

$$\hat{\underline{X}}(t_{i+1}^-) = \begin{bmatrix} e^{-\Delta t/\lambda_D} & 0 & 0 & 0 \\ 0 & e^{-\Delta t/\lambda_D} & 0 & 0 \\ 0 & 0 & e^{-\Delta t/\lambda_A} & 0 \\ 0 & 0 & 0 & e^{-\Delta t/\lambda_A} \end{bmatrix} \hat{\underline{X}}(t_i^+) \quad (54)$$

$$\underline{P}(t_{i+1}^-) = \begin{bmatrix} e^{-\Delta t/\lambda_D} & 0 & 0 & 0 \\ 0 & e^{-\Delta t/\lambda_D} & 0 & 0 \\ 0 & 0 & e^{-\Delta t/\lambda_A} & 0 \\ 0 & 0 & 0 & e^{-\Delta t/\lambda_A} \end{bmatrix} \underline{P}(t_i^+)$$

$$\begin{bmatrix} e^{-\Delta t/\lambda_D} & 0 & 0 & 0 \\ 0 & e^{-\Delta t/\lambda_D} & 0 & 0 \\ 0 & 0 & e^{-\Delta t/\lambda_A} & 0 \\ 0 & 0 & 0 & e^{-\Delta t/\lambda_A} \end{bmatrix}$$

$$+ \begin{bmatrix} \sigma_D^2 (1 - e^{-\frac{2\Delta t}{\lambda_D}}) & 0 & 0 & 0 \\ 0 & \sigma_D^2 (1 - e^{-\frac{2\Delta t}{\lambda_D}}) & 0 & 0 \\ 0 & 0 & \sigma_A^2 (1 - e^{-\frac{2\Delta t}{\lambda_A}}) & 0 \\ 0 & 0 & 0 & \sigma_A^2 (1 - e^{-\frac{2\Delta t}{\lambda_A}}) \end{bmatrix} \quad (55)$$

Measurement Update

Once the state vector and covariance matrix are propagated up to the next sample time, the Kalman filter utilizes this information, along with the measurement vector available, to compute an estimate of the underlying target centroid location. The measurement update equations which are exploited by the Kalman Filter to perform this operation are:

$$\underline{K}(t_i) = \underline{P}(t_i^-) \underline{H}^T(t_i) (\underline{H}(t_i) \underline{P}(t_i^-) \underline{H}(t_i) + \underline{R}(t_i))^{-1} \quad (56)$$

$$\hat{\underline{x}}(t_i^+) = \hat{\underline{x}}(t_i^-) + \underline{K}(t_i) (\underline{z}(t_i) - \underline{h}(\hat{\underline{x}}(t_i^-), t_i)) \quad (57)$$

$$\underline{P}(t_i^+) = \underline{P}(t_i^-) - \underline{K}(t_i) \underline{H}(t_i) \underline{P}(t_i^-) \quad (58)$$

where

$\underline{P}(t_i^-)$ = propagated conditional covariance matrix from filter, before measurement incorporation at time t_i

$\hat{\underline{x}}(t_i^-)$ = propagated state estimate vector from filter

$\underline{K}(t_i)$ = Kalman Filter Gain

$\underline{h}(\hat{\underline{x}}(t_i^-), t_i)$ = non-linear function of intensity measurements at time t_i , as a function of the state estimate

$\underline{H}(t_i) = \frac{\partial \underline{h}(\hat{\underline{x}}(t_i^-), t_i)}{\partial \underline{x}}$ = linear function of intensity measurements

$\underline{z}(t_i)$ = actual measurement vector

To ease the computational burden on the computer, a different form of the measurement update equation called the inverse covariance form is actually used in the computer software (3:26-7). In the conventional form, the calculation of the Kalman Filter Gain requires the inversion of a 64 x 64 matrix for each update, since there are 64 scalar measurements (3:26). However, in the inverse covariance form, only two 4 x 4 inverses are performed to obtain the $\underline{P}(t_i^-)$ and $\underline{P}(t_i^+)$ matrices (3:26-7). The equations for the inverse covariance form are as follows:

$$\underline{P}^{-1}(t_i^+) = \underline{P}^{-1}(t_i^-) + \underline{H}^T(t_i) \underline{R}(t_i) \underline{H}(t_i) \quad (59)$$

$$\underline{P}(t_i^+) = (\underline{P}^{-1}(t_i^+))^{-1} \quad (60)$$

$$\underline{K}(t_i) = \underline{P}(t_i^+) \underline{H}^T(t_i) \underline{R}^{-1}(t_i) \quad (61)$$

$$\underline{\hat{x}}(t_i^+) = \underline{\hat{x}}(t_i^-) + \underline{K}(t_i) (\underline{z}(t_i) - \underline{h}(\underline{\hat{x}}(t_i^-), t_i)) \quad (62)$$

Normally, the non-linear h function and its spatial derivative (linearized H function) which are used in the update equations are explicit in form. However, for this project the non-linear h function is determined in real-time using the FFT, phase shifting and the averaging techniques discussed earlier. While the linearized H function is determined from the non-linear h function using the numerical approximation discussed in Appendix A.

In summary, the measurement update equation is that portion of the Kalman Filter which incorporates the actual intensity measurements to provide a best estimate of the target centroid location. In order to ease the computational burden of inverting a 64 x 64 matrix, the inverse

covariance form of the update equations, which only requires the inversion of two 4×4 matrices, was employed.

III Performance Analysis

The performance analysis for this thesis follows that outlined in the Plan of Attack section. To begin, the validation of the FFT subroutine FOURT not only demonstrated its ability to reconstruct a two-dimensional array of data, but also established a zero level of 10^{-8} . This zero level represents the greatest non-zero value in the IFFT where a zero would be found in the original image array.

The next step involved the development and validation of a subroutine used to perform the negating phase shift. This subroutine called Shift is described in more detail in Appendix D. In short, this subroutine applies the complex conjugate of the resulting linear phase shift from the translation of an image in the space domain to the Fourier transform of this same image. As a result, when the IFFT is taken, an image which is centered in the FOV is the end product. Figure 7 illustrates this process using the 40 urad x 40 urad intensity pattern.

In analyzing the performance of the exponential smoothing technique, a number of parameters were varied using the 3 gaussian pattern as a basis. These parameters included the signal-to-noise ratio, which varied between 10 and 20, and the sigma values for the spread of the gaussian patterns which included 1/4 pixel, 1 pixel, and 3 pixel spreads. The various sigma values provided a spectrum of shapes which ranged from sharply peaked ($\sigma = 1/4$ pixel) to very broad ($\sigma = 3$ pixels). The actual results are displayed in Figures 8 to 13. However, it is important to note that at a signal-to-noise ratio of 20, the pattern is readily identifiable regardless of its shape. However, the average technique does provide some smoothing of the data. At a signal-to-noise ratio of 10, the shape of the

pattern seems to make a difference. For the narrow gaussian patterns ($\sigma = 1/4$ pixel) the pattern is difficult to recognize even after 50 runs. But, for the very wide gaussian pattern the general trend of increasing and decreasing numbers is maintained throughout the process, which may suggest that the filter performance may be better for larger targets. Still, it should be emphasized that this is only a superficial analysis and the more detailed analysis can only be performed once a complete filter simulation has been developed.

In implementing the first truth model, that of a stationary target, a major problem arose. Under ideal conditions (i.e. the Kalman Filter knowing exactly where the target is initially), the filter began to diverge from the known target. This divergence initially appeared at the first measurement update and became progressively worse as each subsequent propagation and measurement update were performed. Initially, it was speculated that there may be a Kalman Filter tuning problem. As a result, various values for the initial covariance matrix (\underline{P}_0) to improve the initial response of the filter, and for the covariance matrices for the dynamic driving noise (\underline{Q}) and the measurement noise (\underline{R}) to improve the steady state response were tried. Nonetheless, no noticeable improvement in the filter's performance resulted from this investigation. Next, it was conjectured that the problem may be within the subroutine UPD which performs the Kalman Filter measurement update. First, the search for a possible sign error or any other fault in the software was performed without any satisfaction. However, upon investigating the calculation of the Kalman filter gain $\underline{K}(t_i)$, it was hypothesized that the forward-backwards difference method used to calculate the linearized h function ($\underline{h}(t_i)$) which in turn is used to calculate the

filter gain, may be the source of the problem. To eliminate any possible concern that the divergence problem may be caused by the generation of the unknown non-linear and linear h functions, the analytic function for the noise-free centered gaussian patterns generated from the subroutine Input 3 was used as the non-linear h function. The analytic spatial derivative of the gaussian pattern in both the x and y directions was next taken and used as the linearized h function. The results of this analysis is presented in Table 1. As can be seen, it is verified that the source of the problem is not due to the generation of the unknown h functions. As a possible solution to this dilemma involving the divergence of the Kalman Filter, the Fourier transform derivative property, which will be discussed in more detail in the Conclusion and Recommendation section, should be implemented.

0	0	0	0	0	0	0	0
0	0	0	0	0	0	0	0
0	0	0	0	0	0	0	0
0	0	0	0	0	0	0	0
0	0	0	0	1	1	0	0
0	0	0	0	1	1	0	0
0	0	0	0	0	0	0	0
0	0	0	0	0	0	0	0

Pattern Shifted
(20 urad, 20 urad)

0	0	0	0	0	0	0	0
0	0	0	0	0	0	0	0
0	0	0	0	0	0	0	0
0	0	0	1	1	0	0	0
0	0	0	1	1	0	0	0
0	0	0	0	0	0	0	0
0	0	0	0	0	0	0	0
0	0	0	0	0	0	0	0

Pattern Resulting From Shift Negation

Figure 7. Results of Shift Routine

0	0	0	0	0	0	0	0
0	0	0	0.455	0.882	0	0	0
0	0	0	0.882	1.71	0	0	0
0	0	0	0	0	0	0	0
0	0	0	0	0	0	0	0
0	0.455	0.882	0	0	0.455	0.882	0
0	0.882	1.71	0	0	0.882	1.71	0
0	0	0	0	0	0	0	0

Figure 8. No Noise $\sigma = 1/4$ pixel $\alpha = 0.1$

0.352	0.283	-0.649	0.519	-0.287	-0.161	-0.427	-0.229
-0.382	-0.222	-0.798	-0.434	1.20	0.263	1.023	0.9622
-0.05	0.287	-0.355	1.53	1.61	1.29	0.138	1.22
-0.156	-0.383	1.71	1.17	0.221	1.26	0.416	1.155
0.731	0.843	-0.042	0.645	-0.176	0.303	1.31	-0.095
-0.082	0.135	-0.323	-0.401	-0.196	-0.336	0.5	-0.129
0.361	0.091	0.36	0.568	1.733	-0.631	1.28	-0.557

Figure 9A. 1st Run $\sigma = 1/4$ Pixel S/N = 10 $\alpha = 0.1$

0.10	0.136	0.0318	0.022	-0.149	-0.218	0.0556	-0.0521
-0.159	-0.232	-0.294	0.444	0.349	0.133	0.183	-0.129
-0.153	0.158	0.684	1.049	0.799	0.223	0.724	0.641
0.087	0.279	0.738	0.572	-0.071	0.158	0.353	0.148
-0.113	-0.131	-0.045	0.127	0.011	0.135	-0.086	0.413
-0.129	0.117	0.319	-0.364	-0.242	-0.121	0.270	-0.081
-0.052	0.398	0.752	0.137	1.148	0.917	1.334	-0.435
0.218	0.293	-0.109	-0.235	0.643	0.133	-0.155	0.133

Figure 9B. 50th Run $\sigma = 1/4$ Pixel S/N = 10 $\alpha = 0.1$

0.352	0.283	-0.649	-0.520	-0.287	-0.161	-0.427	-0.229
-0.382	-0.222	-0.798	-0.207	1.642	0.263	1.023	0.962
-0.049	0.287	0.499	2.41	2.46	1.29	0.992	1.66
-0.156	-0.383	2.15	1.35	0.221	1.26	0.857	1.38
0.731	0.843	-0.042	0.645	-0.176	0.303	1.31	-0.095
-0.083	0.363	1.175	-0.401	-0.196	-0.108	0.941	-0.129
0.361	0.532	1.21	0.568	2.59	0.250	2.14	-0.557
0.297	-0.485	0.378	0.098	2.22	-0.425	-0.467	0.674

Figure 10A. 1st Run $\sigma = 1/4$ Pixel S/N = 20 $\alpha = 0.1$

0.10	0.136	0.032	0.022	-0.149	-0.218	0.056	-0.052
-0.159	-0.231	-0.293	0.683	0.814	0.134	0.183	-0.129
-0.153	0.158	1.49	1.93	1.70	0.223	1.53	1.06
0.087	0.279	1.16	0.787	-0.071	0.158	0.77	0.363
-0.113	-0.131	-0.045	0.127	0.011	0.135	-0.086	0.413
-0.129	0.357	0.784	-0.364	-0.242	0.118	0.734	-0.081
-0.052	0.862	1.65	0.138	1.96	1.80	2.23	-0.434
0.218	0.293	-0.109	-0.235	1.06	0.348	-0.154	0.133

Figure 10B. 50th Run $\sigma = 1/4$ Pixel S/N = 20 $\alpha = 0.1$

12.17	16.46	20.22	22.51	22.73	20.81	17.29	13.03
16.04	21.43	26.08	28.90	29.17	26.82	22.46	17.12
19.84	26.14	31.49	34.72	35.02	32.34	27.33	21.11
23.06	29.97	35.73	39.17	39.49	36.64	31.25	24.47
25.13	32.24	38.08	41.51	41.84	38.99	33.55	26.60
25.52	32.39	37.94	41.16	41.47	38.79	33.64	26.94
23.95	30.14	35.07	37.92	38.18	35.83	31.26	25.23
20.61	25.78	29.86	32.18	32.40	30.48	26.71	21.69

Figure 11. No Noise IMAX = 20 $\sigma = 3$ pixels

5.51	7.51	7.71	11.22	11.11	10.36	8.79	6.81
8.16	11.49	12.90	13.33	15.83	13.81	10.42	9.17
9.60	13.16	15.75	15.41	18.81	16.96	11.75	9.83
10.51	15.21	18.73	19.04	19.77	19.11	14.41	13.36
14.14	15.93	20.27	20.42	20.80	20.38	16.31	13.03
13.80	16.33	19.86	21.89	20.67	21.17	17.56	12.62
12.0	15.0	17.91	20.10	19.82	19.27	15.13	13.06
11.31	13.51	16.26	16.04	16.10	13.79	10.31	10.69

Figure 12A. 1st Run $\sigma = 3$ pixels $S/N = 10$ $\alpha = 0.1$

3.304	4.472	5.355	5.951	5.838	5.264	4.608	3.378
4.064	10.55	12.89	15.03	15.24	14.81	13.16	10.48
5.071	13.01	15.57	17.79	18.16	17.71	15.41	12.92
6.16	14.55	17.69	19.85	20.14	19.55	17.14	14.04
6.51	14.66	17.92	20.29	20.93	20.23	17.76	15.05
6.59	14.20	17.24	19.15	20.03	19.12	17.12	14.11
6.25	12.87	15.56	17.78	18.68	17.69	16.12	12.40
5.65	11.13	13.07	14.59	15.66	14.78	13.05	10.92

Figure 12B. 50th Run $\sigma = 3$ pixels $S/N = 10$ $\alpha = 0.1$

11.59	15.74	17.82	22.48	22.47	20.77	17.44	13.32
16.17	22.20	25.94	27.79	30.41	27.22	21.66	17.73
19.52	26.23	31.50	32.77	36.32	33.13	25.41	20.59
22.04	30.19	36.60	38.62	39.51	37.43	30.04	25.60
26.70	32.05	39.31	41.18	41.72	39.88	33.09	26.32
26.55	32.53	38.83	42.47	41.40	40.56	34.37	26.09
23.97	30.06	35.44	39.06	38.91	37.18	30.76	25.68
21.61	26.40	31.19	32.13	32.30	29.03	23.66	21.53

Figure 13A. 1st Run $\sigma = 3$ pixels S/N = 20 $\alpha = 0.1$

6.51	8.81	10.67	11.87	11.82	10.74	9.16	6.81
8.29	21.32	26.08	29.85	30.59	29.49	26.14	21.09
10.29	25.87	31.26	35.41	36.42	35.20	30.91	25.61
12.23	28.81	35.06	39.35	40.36	38.94	34.35	28.15
13.12	29.44	35.89	40.45	41.85	40.32	35.61	29.83
13.31	28.52	34.63	38.66	40.29	38.61	34.43	28.29
12.56	25.80	31.26	35.41	37.03	35.34	31.80	25.23
11.07	21.97	26.24	29.41	31.10	29.65	26.26	21.70

Figure 13B. 50th Run $\sigma = 3$ pixels S/N = 20 $\alpha = 0.1$

Measurement Update No.	Correct		Results		Unknown h Func' is		Known Non-linear h Function		Known h Functions	
	$\underline{x_D}$	$\underline{y_D}$	$\underline{x_D}$	$\underline{y_D}$	$\underline{x_D}$	$\underline{y_D}$	$\underline{x_D}$	$\underline{y_D}$	$\underline{x_D}$	$\underline{y_D}$
1	0.0	0.0	-0.565	0.934	-0.0028	0.449	0.00137	0.4178		
5	0.0	0.0	***	8.307	-4.82	0.126	-4.608	0.0163		
10	0.0	0.0	***	57.09	***	***	***	***		
20	0.0	0.0	***	***	***	***	***	***		
50	0.0	0.0	***	***	***	***	***	***		

*** Absolute value exceeds 100

Table 1. Divergence Analysis

IV Conclusions and Recommendations

In conclusion, this thesis did not accomplish nearly as much as anticipated at the beginning of the project. However, a number of milestones were realized. To name a few, the digital implementation of a negating phase shift, the validation of the FOURT subroutine, and the implementation of the exponential smoothing technique were highlights of this project. Since the investigation of the deterministic stationary truth model identified a possible problem with the forward-backward difference approximation, the deterministic constant velocity and stochastic truth models were not analyzed.

Although some analysis was accomplished with this project, more is needed. To begin, the arbitrary assumption of padding the input array with 8 additional rows and columns of zeroes could be investigated in more detail to determine if little distortion results in using less zeroes. In addition, a further extension on the analysis of the averaging technique would involve not only a further investigation of its dependency on the image shape, but also an investigation of how the filter's performance is affected when the steady state value of the smoothing constant α is varied. Another modification to the computer algorithm that could be made deals with the sampling scheme described in Appendix A. A more unbiased and resolvable sampling scheme could be implemented. However, the addition of the Fourier transform derivative property would be the most important modification to the existing computer software, since it provides the best hope of solving the filter divergence problem. Analytically, the spatial derivative of the non-linear h function represents the linearized h function. This spatial

derivative could be more precisely calculated by using the following Fourier property:

$$\mathcal{T} \left\{ \frac{\partial h(x,y)}{\partial x} \right\} = +j2\pi f_x H(f_x, f_y) \quad (63)$$

$$\mathcal{T} \left\{ \frac{\partial h(x,y)}{\partial y} \right\} = j2\pi f_y H(f_x, f_y) \quad (17:314) \quad (64)$$

As a possible plan of attack for future research, the following steps may be taken. First and most importantly, the filter divergence problem must be solved, hopefully with the use of the Fourier Transform divergence property. Next, the deterministic constant velocity and stochastic truth models should be employed keeping in mind that the normal robustness that is characteristic of Kalman filters may not be possible since the negating phase shift requires extremely accurate estimates of the target location. Once this has been performed, the filter performance can be evaluated based on changes to the zero padding of the input array, changes to the sampling scheme of the same input array, and variation to the steady state smoothing constant.

Bibliography

1. Bass M., Copley S., Beck D. G., and Wallace R. J. "Laser Assisted Hot Spot Maching," Proceeding of the Symposium on Laser-Solid Interactions and Laser Processing, 205-11, Boston, Massachusetts, November 27 - December 1, 1978.
2. Pertsov, O. L. "Biophysical Aspects of the Use of Lasers in Medical Research," Soviet Journal of Optical Technology, 46: 360-66 (June 1979).
3. Mercier, Daniel E. "An Extended Kalman Filter for Use in a Shared Aperture Medium Range Tracker," M.S. Thesis, Air Force Institute of Technology, Wright-Patterson AFB, Ohio, December 1978.
4. Maybeck, Peter S. "The Kalman Filter an Introduction for Potential Users," June 1972.
5. Harnly, Douglas A. and Jensen, Robert L. "An Adaptive Distributed-Measurement Extended Kalman Filter for a Short Range Tracker," M.S. Thesis, Air Force Institute of Technology, Wright-Patterson AFB, Ohio, December 1979.
6. Hanuise, Guy. "Image Processing by Computer," 1975.
7. Goodman, Joseph W. Introduction to Fourier Optics. McGraw-Hill Book Company, 1968.
8. Fukunaga, Keinosuke. Introduction to Statistical Pattern Recognition. New York: Academic Press Incorporated, 1972.
9. Oppenheim, Alan V. and Schafer, Ronald W. Digital Signal Processing. New Jersey: Prentice-Hall Incorporated, 1975.
10. Cooley J. W., Lewis P. A., and Welch P. D. "Historical Notes on the Fast Fourier Transform," IEEE Transactions on Audio and Electroacoustics, Volume Au-15 Number 2: 76-79 (June 1967).
11. Bush, Larry F. "The Design of an Optimum Alphanumeric Symbol Set for Cockpit Displays," M.S. Thesis, Air Force Institute of Technology, Wright-Patterson AFB, December 1977.
12. Bedworth, David D. Industrial Systems Planning, Analysis, Control. New York: The Ronald Press Company, 1973.
13. Maybeck, Peter S., Professor of Electrical Engineering. Personal interview. Air Force Institute of Technology, Wright-Patterson AFB, Ohio, August 1, 1980.
14. The Analytic Sciences Corporation. Advanced Adaptive Optics Control Techniques. TR-996-1. Prepared for the Air Force Weapons Laboratory, Kirtland Air Force Base, New Mexico, January 6, 1978.

15. Hogge, C. B. and Butts, R. R. "Frequency Spectra for the Geometric Representation of Wavefront Distortions Due to Atmospheric Turbulence," IEEE Transactions on Antenna and Propagation, Vol. AP-24, No. 2, March 1976. (Program supplied by authors).
16. Maybeck, Peter S. Stochastic Models, Estimation, and Control Volume I. New York: Academic Press Incorporated, 1979.
17. Gaskill, Jack D. Linear Systems, Fourier Transforms, and Optics. John Wiley and Sons, 1978.
18. Hornbeck, Robert W. Numerical Methods. Quantum Publishers, Incorporated, 1975.

APPENDIX A

Numerical Approximation

In the development of this thesis project, two numerical approximations were used. In generating the measurement vector $\underline{z}(t_i)$, the first approximation involved computing the average intensity over each pixel. Algebraically, the component of the $\underline{z}(t_i)$ vector corresponding to a particular pixel is

$$z_{jk}(t_i) = \frac{1}{A_p} \iint_{\substack{\text{region of} \\ \text{jk}^{\text{th}} \text{ pixel}}} I_{\text{target}}(x,y,t_i) dx dy + v_{jk}(t_i) \quad (65)$$

where A_p = area of one pixel

$I(x,y,t_i)$ = two-dimensional intensity pattern

$v_{jk}(t_i)$ = noise effect on the jk^{th} pixel

$z_{jk}(t_i)$ = actual measurement from jk^{th} pixel

Since a simple functional form of the intensity pattern that can be analytically integrated is not available, the exact integration of equation 65 cannot be performed. Instead, 25 sample points from each pixel will be taken and averaged to provide the average intensity over the pixel. The exact locations are given in Figure 14 below. It should be noted that samples are taken along the top and left edge of the pixel of interest so that duplicate sampling does not occur along the edges. In other words, the right edge becomes the sampled left edge for the next pixel to the right, while the bottom edge becomes the sampled top edge for the pixel just below. The selection of this sampling scheme was arbitrary. In follow-on projects, more samples from different locations may be taken to provide better resolution and thus more sensitivity

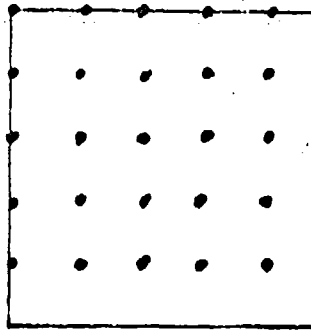


Figure 14. Pixel Sampling Scheme

to the movement of the intensity pattern from one sample period to another.

The second approximation, which is indirectly tied to the first, involves the generation of the linearized h function. Since an explicit analytical form of the non-linear h function is not available, an exact differentiation of this non-linear function to provide a linearized function cannot be performed. Instead, a numerical approximation known as the Forward-Backwards Difference Method is used (18:16-17). A familiar numerical method used in finite difference calculus, this technique is used to compute the derivative of a function to any higher order. However, to compute the first order spatial derivative for a particular pixel, the pixel values, along the direction for which the spatial derivative is taken, just before and just after the pixel of interest is used. The values are subtracted from each other and divided by the distance between each other (i.e. 40 μ rad). For the pixels located along the edges for which the pixel just before or just after does not exist, either just a forward or just a backwards difference is taken. To be more specific, the value of the pixel itself is subtracted from

either the value of the pixel just before or just after, whichever is available, and divided by the distance between the two (i.e. 20 urad). For example, referring to Figure 5, Pixel Numbering Scheme, if the spatial derivative in the x direction for pixel number 29 is to be computed, the value for pixel 28 is subtracted from the value for pixel 30 and divided by 40. However, along the edge, just a forward or backward difference has to be calculated. For instance, to find the spatial derivative in the y direction for pixel number 3, the value for pixel 3 is subtracted from the value for pixel 11 and divided by 20.

APPENDIX B

Coordinate System for 8 x 8 Input Array

The development of a coordinate system to use throughout this project was critical. The 8 x 8 input array represents an 8 x 8 FLIR array whose individual pixel FOV is 20 urad x 20 urad and system FOV is 160 urad x 160 urad. With the additional 8 rows and columns of zeroes (see Fourier Transform section), the resulting 24 x 24 array of data actually represents a coordinate system that is 480 urad x 480 urad with the (0,0) coordinate in the upper left hand corner, x increasing from left to right and y increasing from top to bottom (Figure 15).

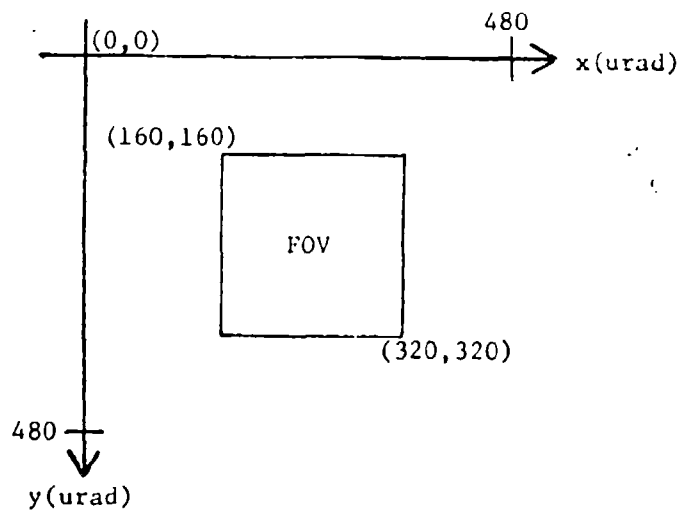


Figure 15. Coordinate System for Input Array

APPENDIX C

Input Patterns

Although the development of the Extended Kalman Filter for this thesis assumed no a priori knowledge concerning the exact algebraic form of the intensity pattern, three different intensity patterns were developed to provide the measurement vector $\underline{z}(t_i)$ necessary to verify the performance of the Kalman Filter. The actual computer subroutines (Input 1, Input 2, Input 3) are described in Appendix D. However, the three input patterns are a 40 x 40 constant intensity block, 3 constant height cylinder patterns, and 3 gaussian profiles. Figures 16a,b,c illustrate how the centered patterns would appear on the FLIR array. Figures 17a,b,c show the resulting noise-free values for the average intensity per pixel. The selection of these three patterns is significant, since the 40 x 40 pattern provides a very pronounced difference between zero and non-zero values, while the 3 cylinder pattern once again provides a pronounced difference between zero and non-zero values but is closer to simulating a multiple-hot-spot target, while the 3 gaussian profiles provide the best representation of the multiple-hot-spot targets.

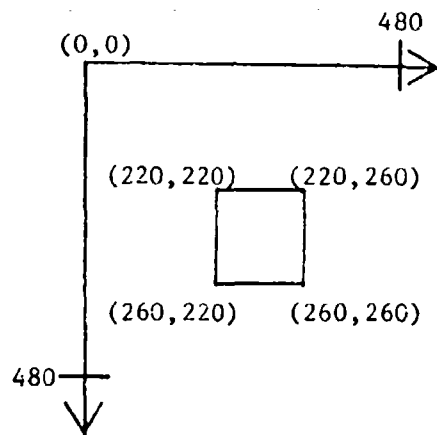


Figure 16a. 40 x 40 Constant Intensity

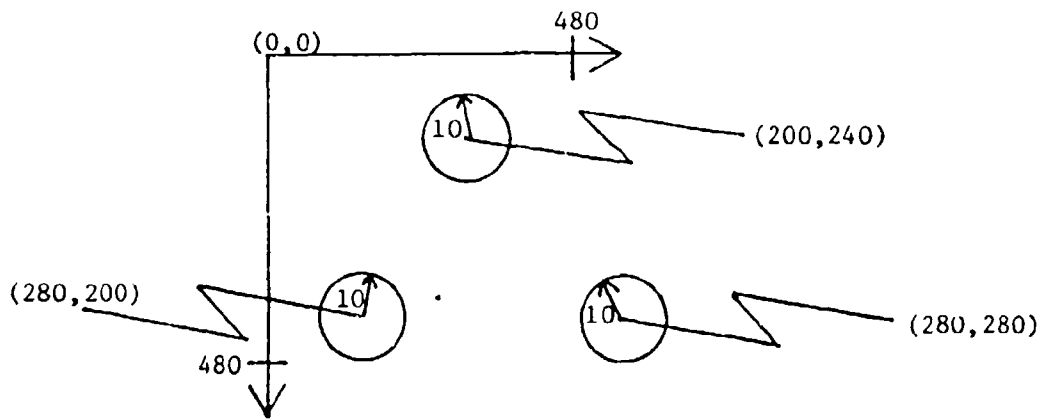


Figure 16b. 3 Constant Height Cylinders

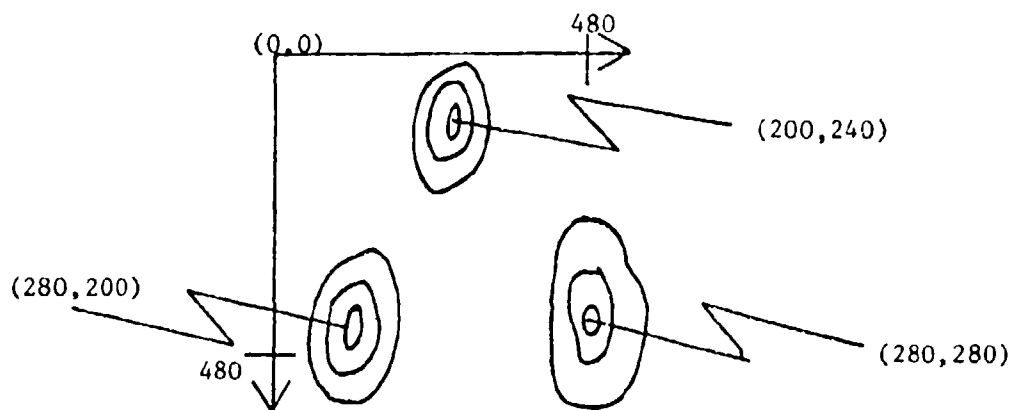


Figure 16c. 3 Gaussian Profiles

0	0	0	0	0	0	0	0
0	0	0	0	0	0	0	0
0	0	0	0	0	0	0	0
0	0	0	1	1	0	0	0
0	0	0	1	1	0	0	0
0	0	0	0	0	0	0	0
0	0	0	0	0	0	0	0
0	0	0	0	0	0	0	0

Figure 17a. Discrete 40 x 40 Constant Intensity

0	0	0	0	0	0	0	0
0	0	0	0	0	0	0	0
0	0	0	0.2	0.32	0	0	0
0	0	0	0.12	0.2	0	0	0
0	0	0	0	0	0	0	0
0	0.2	0.32	0	0	0.2	0.32	0
0	0.12	0.2	0	0	0.12	0.2	0
0	0	0	0	0	0	0	0

Figure 17b. Discrete 3 Constant Height Cylinders

0	0	0	0	0	0	0	0
0	0	0	0.045	0.0881	0	0	0
0	0	0	0.0881	0.171	0	0	0
0	0	0	0	0	0	0	0
0	0	0	0	0	0	0	0
0	0.045	0.0881	0	0	0.045	0.0881	0
0	0.0881	0.171	0	0	0.0881	0.171	0
0	0	0	0	0	0	0	0

$$\sigma = 1/4 \text{ Pixel}$$

Figure 17c. Discrete 3 Gaussian Profiles

APPENDIX D
Computer Software

This appendix contains the Fortran computer software used for this project. The computer software only reflects the use of the stationary target truth model. Since some models were used from previous thesis, there may be some duplication of their work within this software. This program was written for use on the CDC 6600 Fortran IV compiler.


```

11 IF(SIGMA2)GO TO 72
12 IF(SIGMA3)GO TO 73
13 PRINT,REMARKS IN IDENTIFYING NOISE TYPE,
14 " WILL ASSURE NO NOISE CORRUPTION IN SIMULATION"
15 STOP
16 GO TO 71
17 CALL VOICE(CORRELATION COEFFICIENT MATRIX
18 " SPATIAL NOISE")
19 PRINT,REMARKS SPATIAL NOISE="SIGMA4"
20 CALL VOICE(C(1),C(2),C(3),C(4),C(5))
21 PRINT,REMARKS "CORRELATION COEFFICIENTS"
22 PRINT, C(1),C(2),C(3),C(4),C(5)
23 CALL SPIN(C,SIGMA4,SIN,PHI)
24 CALL NOISE(CORRELATION COEFFICIENT MATRIX
25 " TEMPORAL NOISE")
26 PRINT,REMARKS "TEMPORAL NOISE="SIGMA4"
27 PRINT,REMARKS "RELATION TIME FOR TEMPORAL NOISE",TAU
28 SIGMA7=SIGMA7*(1.-EXP(-2./TAU))
29 DO 77 I=1,N
30 PAREN(I)=EXP(-I/TAU)
31 COMPUTE
32 C(1)=0.
33 C(2)=0.
34 C(3)=0.
35 C(4)=0.
36 C(5)=0.
37 CALL VOICE(SIGMA7,SIN,PHI)
38 CALL NOISE(CORRELATION COEFFICIENTS)
39 PRINT,REMARKS "RELATION TIME",TAU
40 SIGMA7=SIGMA7*(1.-EXP(-2./TAU))
41 DO 77 I=1,N
42 PAREN(I)=EXP(-I/TAU)
43 COMPUTE
44 CALL VOICE(CORRELATION COEFFICIENT MATRIX
45 " SPATIAL AND TEMPORAL NOISE",SIGMA7)
46 PRINT,REMARKS "CORRELATION COEFFICIENTS"
47 PRINT, C(1),C(2),C(3),C(4),C(5)
48 CALL SPIN(C,SIGMA7,SIN,PHI)
49 CALL NOISE(CORRELATION COEFFICIENT MATRIX
50 " STATE TRANSITION MATRIX")
51 PRINT,REMARKS "STATE TRANSITION MATRIX"
52 PRINT, PH(I,J)=EXP(-DELTA/TAU)
53 DO 77 J=1,N
54 DO 77 I=1,N
55 PAREN(I)=EXP(-I/TAU)
56 COMPUTE
57 CALL VOICE(CORRELATION COEFFICIENT MATRIX
58 " STATE TRANSITION MATRIX")
59 PRINT,REMARKS "STATE TRANSITION MATRIX"
60 PRINT, PH(I,J),J=1,N
61 PRINT, I=1,N
62 STOP

```

Best Available Copy

```

170  C0(L,1)=12.
      C0(L,2)=D(1,1)
      C0(L,3)=2*GPA1*(C0(L,2)*EXP(-2.*DILT/TAUP))
      C0(L,4)=D(2,2)
      PAET=MOD(PAET-1)

```

```

22  CALL F1(C0(I,J),J=1,4)
      CONTINUE
      K=K+1

```

```

23  IF(K.GT.1) GO TO 24
      SUFF=KX-GENRY
      SUFF=GENY-GENY

```

```

24  C0(I,1)=SUFF
      SUFF=V(I)+YE(I)
      SUFF=X(I)+Y(I)
      CALL ACC(SUFF)
      CALL ACC(SUFF)

```

```

25  I=I+1
      CALL F0(I,PAET,NO,NOIM,ISIGH,IFORM,MCRC)
      CALL SUBT(UB,UB,SUFF,SUFF)

```

```

26  F1=C0(I,1)+C0(I,2)
      C0(I,3)=F1*(1-DILT/TAUP)
      C0(I,4)=F1*(1-DILT/TAUP)

```

```

27  IF(C0(I,3).GT.0) GO TO 28
      I=I+1

```

```

28  CALL MAIN CONTINUE WITH FAST DATA USING EXPONENTIAL SMOOTHING

```

```

29  DO 1 I=1,N
      DO 2 J=1,4

```

```

30  C0(I,J)=C0(I,J)+((C0(I,J)) - ((C0(I,J)-4)*DATA2(I,J)))
      CONTINUE

```

```

31  CALL F0(I,PAET,NO,NOIM,ISIGH,IFORM,MCRC)
      DO 2 J=1,4

```

```

32  C0(I,J)=DATA2(I,J)/101
      IF(C0(I,J).LT.1E-10) DATA2(I,J)=0.

```

```

33  IF(C0(I,J).LT.1E-10) DATA2(I,J)=0.
      CONTINUE

```

```

34  CALL F0(I,PAET,NO,NOIM,ISIGH,IFORM,MCRC)
      DO 2 J=1,4

```

```

35  C0(I,J)=DATA2(I,J)/101
      IF(C0(I,J).LT.1E-10) DATA2(I,J)=0.

```

```

36  CALL F0(I,PAET,NO,NOIM,ISIGH,IFORM,MCRC)
      DO 2 J=1,4

```

```

37  C0(I,J)=DATA2(I,J)/101
      IF(C0(I,J).LT.1E-10) DATA2(I,J)=0.

```

```

38  CALL F0(I,PAET,NO,NOIM,ISIGH,IFORM,MCRC)
      DO 2 J=1,4

```

```

39  C0(I,J)=DATA2(I,J)/101
      IF(C0(I,J).LT.1E-10) DATA2(I,J)=0.

```

```

40  CALL F0(I,PAET,NO,NOIM,ISIGH,IFORM,MCRC)
      DO 2 J=1,4

```

```

41  C0(I,J)=DATA2(I,J)/101
      IF(C0(I,J).LT.1E-10) DATA2(I,J)=0.

```

```

42  CALL F0(I,PAET,NO,NOIM,ISIGH,IFORM,MCRC)
      DO 2 J=1,4

```



```

X=(J-1)*2... + (K2-1)*4...
SYMBOLIC REFERENCE MAP (REI)
ENTRY POINTS
3 STATEM1

```

Best Available Copy

SYMBOLIC REFERENCE MAP (REI)

ENTRY POINTS

VARIABLES	SM	TYPE	DECLARATION
201 X	REAL	REAL	F.P.
202 Y	REAL	REAL	F.P.
203 I	DATA1	DATA1	
204 J	DATA1	DATA1	
205 K	DATA1	DATA1	
206 L	DATA1	DATA1	
207 M	DATA1	DATA1	
208 N	DATA1	DATA1	
209 O	DATA1	DATA1	
210 P	DATA1	DATA1	
211 Q	DATA1	DATA1	
212 R	DATA1	DATA1	
213 S	DATA1	DATA1	
214 T	DATA1	DATA1	
215 U	DATA1	DATA1	
216 V	DATA1	DATA1	
217 W	DATA1	DATA1	
218 X	DATA1	DATA1	
219 Y	DATA1	DATA1	
220 Z	DATA1	DATA1	

FILE NAMES

STATEMENT LABELS

LOGS	LABEL	INDEX	START-TO	LENGTH	PROPERTIES
150	20	T	22 72	547	NOT INNER
74	32	J	52 71	519	NOT INNER
1..	32	KL	7- 19	373	NOT INNER
122		K2	52 18	219	

137 5
62 36
64 33

140 5
56 31
76 34

NOT INNER
NOT INNER
NOT INNER

UPI

```

1 SUBROUTINE INTEGRATION(X1,UF1,UF2,N,IMAX,CENX,CFNY)
2  DIMENSION OF(1:IMAX),IMAX(3)
3  COMPLEX DATA
4  REAL X1,UF1,UF2,IMAX
5  300 READ LEVEL IS (LIVED) INTO 25 PIECES FOR INTEGRATION

```

```

6  OX1=0.0 + OF1
7  OY1=0.0 + OF2
8  OX2=0.0 + OF3
9  OY2=0.0 + OF4
10 OX3=0.0 + OF5
11 OY3=0.0 + OF6
12 OX4=0.0 + OF7
13 OY4=0.0 + OF8
14 OX5=0.0 + OF9
15 OY5=0.0 + OF10
16 OX6=0.0 + OF11
17 OY6=0.0 + OF12
18 OX7=0.0 + OF13
19 OY7=0.0 + OF14
20 OX8=0.0 + OF15
21 OY8=0.0 + OF16
22 OX9=0.0 + OF17
23 OY9=0.0 + OF18
24 OX10=0.0 + OF19
25 OY10=0.0 + OF20

```

```

26 3000 COMPARISON OF X AND Y VALUES
27  V=(X1-0.0)**2 + (Y1-0.0)**2
28  V=(X2-0.0)**2 + (Y2-0.0)**2
29  V=(X3-0.0)**2 + (Y3-0.0)**2
30  V=(X4-0.0)**2 + (Y4-0.0)**2
31  V=(X5-0.0)**2 + (Y5-0.0)**2
32  V=(X6-0.0)**2 + (Y6-0.0)**2
33  V=(X7-0.0)**2 + (Y7-0.0)**2
34  V=(X8-0.0)**2 + (Y8-0.0)**2
35  V=(X9-0.0)**2 + (Y9-0.0)**2
36  V=(X10-0.0)**2 + (Y10-0.0)**2

```

```

37 3000 EVALUATION OF FX
38  V=(X1-0.0)**2 + (Y1-0.0)**2
39  V=(X2-0.0)**2 + (Y2-0.0)**2
40  V=(X3-0.0)**2 + (Y3-0.0)**2
41  V=(X4-0.0)**2 + (Y4-0.0)**2
42  V=(X5-0.0)**2 + (Y5-0.0)**2
43  V=(X6-0.0)**2 + (Y6-0.0)**2
44  V=(X7-0.0)**2 + (Y7-0.0)**2
45  V=(X8-0.0)**2 + (Y8-0.0)**2
46  V=(X9-0.0)**2 + (Y9-0.0)**2
47  V=(X10-0.0)**2 + (Y10-0.0)**2

```

```

48 3000 EVALUATION OF NUMERATOR FOR CENTROID LOCATION
49  V=(X1-0.0)**2 + (Y1-0.0)**2
50  V=(X2-0.0)**2 + (Y2-0.0)**2
51  V=(X3-0.0)**2 + (Y3-0.0)**2
52  V=(X4-0.0)**2 + (Y4-0.0)**2
53  V=(X5-0.0)**2 + (Y5-0.0)**2
54  V=(X6-0.0)**2 + (Y6-0.0)**2
55  V=(X7-0.0)**2 + (Y7-0.0)**2
56  V=(X8-0.0)**2 + (Y8-0.0)**2
57  V=(X9-0.0)**2 + (Y9-0.0)**2
58  V=(X10-0.0)**2 + (Y10-0.0)**2

```

```

59  V=(X1-0.0)**2 + (Y1-0.0)**2
60  V=(X2-0.0)**2 + (Y2-0.0)**2
61  V=(X3-0.0)**2 + (Y3-0.0)**2
62  V=(X4-0.0)**2 + (Y4-0.0)**2
63  V=(X5-0.0)**2 + (Y5-0.0)**2
64  V=(X6-0.0)**2 + (Y6-0.0)**2
65  V=(X7-0.0)**2 + (Y7-0.0)**2
66  V=(X8-0.0)**2 + (Y8-0.0)**2
67  V=(X9-0.0)**2 + (Y9-0.0)**2
68  V=(X10-0.0)**2 + (Y10-0.0)**2

```

```

69  V=(X1-0.0)**2 + (Y1-0.0)**2
70  V=(X2-0.0)**2 + (Y2-0.0)**2
71  V=(X3-0.0)**2 + (Y3-0.0)**2
72  V=(X4-0.0)**2 + (Y4-0.0)**2
73  V=(X5-0.0)**2 + (Y5-0.0)**2
74  V=(X6-0.0)**2 + (Y6-0.0)**2
75  V=(X7-0.0)**2 + (Y7-0.0)**2
76  V=(X8-0.0)**2 + (Y8-0.0)**2
77  V=(X9-0.0)**2 + (Y9-0.0)**2
78  V=(X10-0.0)**2 + (Y10-0.0)**2

```

```

79  V=(X1-0.0)**2 + (Y1-0.0)**2
80  V=(X2-0.0)**2 + (Y2-0.0)**2
81  V=(X3-0.0)**2 + (Y3-0.0)**2
82  V=(X4-0.0)**2 + (Y4-0.0)**2
83  V=(X5-0.0)**2 + (Y5-0.0)**2
84  V=(X6-0.0)**2 + (Y6-0.0)**2
85  V=(X7-0.0)**2 + (Y7-0.0)**2
86  V=(X8-0.0)**2 + (Y8-0.0)**2
87  V=(X9-0.0)**2 + (Y9-0.0)**2
88  V=(X10-0.0)**2 + (Y10-0.0)**2

```

```

89  V=(X1-0.0)**2 + (Y1-0.0)**2
90  V=(X2-0.0)**2 + (Y2-0.0)**2
91  V=(X3-0.0)**2 + (Y3-0.0)**2
92  V=(X4-0.0)**2 + (Y4-0.0)**2
93  V=(X5-0.0)**2 + (Y5-0.0)**2
94  V=(X6-0.0)**2 + (Y6-0.0)**2
95  V=(X7-0.0)**2 + (Y7-0.0)**2
96  V=(X8-0.0)**2 + (Y8-0.0)**2
97  V=(X9-0.0)**2 + (Y9-0.0)**2
98  V=(X10-0.0)**2 + (Y10-0.0)**2

```

```

99  V=(X1-0.0)**2 + (Y1-0.0)**2
100 V=(X2-0.0)**2 + (Y2-0.0)**2
101 V=(X3-0.0)**2 + (Y3-0.0)**2
102 V=(X4-0.0)**2 + (Y4-0.0)**2
103 V=(X5-0.0)**2 + (Y5-0.0)**2
104 V=(X6-0.0)**2 + (Y6-0.0)**2
105 V=(X7-0.0)**2 + (Y7-0.0)**2
106 V=(X8-0.0)**2 + (Y8-0.0)**2
107 V=(X9-0.0)**2 + (Y9-0.0)**2
108 V=(X10-0.0)**2 + (Y10-0.0)**2

```

```

109 V=(X1-0.0)**2 + (Y1-0.0)**2
110 V=(X2-0.0)**2 + (Y2-0.0)**2
111 V=(X3-0.0)**2 + (Y3-0.0)**2
112 V=(X4-0.0)**2 + (Y4-0.0)**2
113 V=(X5-0.0)**2 + (Y5-0.0)**2
114 V=(X6-0.0)**2 + (Y6-0.0)**2
115 V=(X7-0.0)**2 + (Y7-0.0)**2
116 V=(X8-0.0)**2 + (Y8-0.0)**2
117 V=(X9-0.0)**2 + (Y9-0.0)**2
118 V=(X10-0.0)**2 + (Y10-0.0)**2

```

```

119 V=(X1-0.0)**2 + (Y1-0.0)**2
120 V=(X2-0.0)**2 + (Y2-0.0)**2
121 V=(X3-0.0)**2 + (Y3-0.0)**2
122 V=(X4-0.0)**2 + (Y4-0.0)**2
123 V=(X5-0.0)**2 + (Y5-0.0)**2
124 V=(X6-0.0)**2 + (Y6-0.0)**2
125 V=(X7-0.0)**2 + (Y7-0.0)**2
126 V=(X8-0.0)**2 + (Y8-0.0)**2
127 V=(X9-0.0)**2 + (Y9-0.0)**2
128 V=(X10-0.0)**2 + (Y10-0.0)**2

```

```

129 V=(X1-0.0)**2 + (Y1-0.0)**2
130 V=(X2-0.0)**2 + (Y2-0.0)**2
131 V=(X3-0.0)**2 + (Y3-0.0)**2
132 V=(X4-0.0)**2 + (Y4-0.0)**2
133 V=(X5-0.0)**2 + (Y5-0.0)**2
134 V=(X6-0.0)**2 + (Y6-0.0)**2
135 V=(X7-0.0)**2 + (Y7-0.0)**2
136 V=(X8-0.0)**2 + (Y8-0.0)**2
137 V=(X9-0.0)**2 + (Y9-0.0)**2
138 V=(X10-0.0)**2 + (Y10-0.0)**2

```

```

139 V=(X1-0.0)**2 + (Y1-0.0)**2
140 V=(X2-0.0)**2 + (Y2-0.0)**2
141 V=(X3-0.0)**2 + (Y3-0.0)**2
142 V=(X4-0.0)**2 + (Y4-0.0)**2
143 V=(X5-0.0)**2 + (Y5-0.0)**2
144 V=(X6-0.0)**2 + (Y6-0.0)**2
145 V=(X7-0.0)**2 + (Y7-0.0)**2
146 V=(X8-0.0)**2 + (Y8-0.0)**2
147 V=(X9-0.0)**2 + (Y9-0.0)**2
148 V=(X10-0.0)**2 + (Y10-0.0)**2

```

```

149 V=(X1-0.0)**2 + (Y1-0.0)**2
150 V=(X2-0.0)**2 + (Y2-0.0)**2
151 V=(X3-0.0)**2 + (Y3-0.0)**2
152 V=(X4-0.0)**2 + (Y4-0.0)**2
153 V=(X5-0.0)**2 + (Y5-0.0)**2
154 V=(X6-0.0)**2 + (Y6-0.0)**2
155 V=(X7-0.0)**2 + (Y7-0.0)**2
156 V=(X8-0.0)**2 + (Y8-0.0)**2
157 V=(X9-0.0)**2 + (Y9-0.0)**2
158 V=(X10-0.0)**2 + (Y10-0.0)**2

```

```

159 V=(X1-0.0)**2 + (Y1-0.0)**2
160 V=(X2-0.0)**2 + (Y2-0.0)**2
161 V=(X3-0.0)**2 + (Y3-0.0)**2
162 V=(X4-0.0)**2 + (Y4-0.0)**2
163 V=(X5-0.0)**2 + (Y5-0.0)**2
164 V=(X6-0.0)**2 + (Y6-0.0)**2
165 V=(X7-0.0)**2 + (Y7-0.0)**2
166 V=(X8-0.0)**2 + (Y8-0.0)**2
167 V=(X9-0.0)**2 + (Y9-0.0)**2
168 V=(X10-0.0)**2 + (Y10-0.0)**2

```

```

169 V=(X1-0.0)**2 + (Y1-0.0)**2
170 V=(X2-0.0)**2 + (Y2-0.0)**2
171 V=(X3-0.0)**2 + (Y3-0.0)**2
172 V=(X4-0.0)**2 + (Y4-0.0)**2
173 V=(X5-0.0)**2 + (Y5-0.0)**2
174 V=(X6-0.0)**2 + (Y6-0.0)**2
175 V=(X7-0.0)**2 + (Y7-0.0)**2
176 V=(X8-0.0)**2 + (Y8-0.0)**2
177 V=(X9-0.0)**2 + (Y9-0.0)**2
178 V=(X10-0.0)**2 + (Y10-0.0)**2

```

```

179 V=(X1-0.0)**2 + (Y1-0.0)**2
180 V=(X2-0.0)**2 + (Y2-0.0)**2
181 V=(X3-0.0)**2 + (Y3-0.0)**2
182 V=(X4-0.0)**2 + (Y4-0.0)**2
183 V=(X5-0.0)**2 + (Y5-0.0)**2
184 V=(X6-0.0)**2 + (Y6-0.0)**2
185 V=(X7-0.0)**2 + (Y7-0.0)**2
186 V=(X8-0.0)**2 + (Y8-0.0)**2
187 V=(X9-0.0)**2 + (Y9-0.0)**2
188 V=(X10-0.0)**2 + (Y10-0.0)**2

```

```

189 V=(X1-0.0)**2 + (Y1-0.0)**2
190 V=(X2-0.0)**2 + (Y2-0.0)**2
191 V=(X3-0.0)**2 + (Y3-0.0)**2
192 V=(X4-0.0)**2 + (Y4-0.0)**2
193 V=(X5-0.0)**2 + (Y5-0.0)**2
194 V=(X6-0.0)**2 + (Y6-0.0)**2
195 V=(X7-0.0)**2 + (Y7-0.0)**2
196 V=(X8-0.0)**2 + (Y8-0.0)**2
197 V=(X9-0.0)**2 + (Y9-0.0)**2
198 V=(X10-0.0)**2 + (Y10-0.0)**2

```

```

199 V=(X1-0.0)**2 + (Y1-0.0)**2
200 V=(X2-0.0)**2 + (Y2-0.0)**2
201 V=(X3-0.0)**2 + (Y3-0.0)**2
202 V=(X4-0.0)**2 + (Y4-0.0)**2
203 V=(X5-0.0)**2 + (Y5-0.0)**2
204 V=(X6-0.0)**2 + (Y6-0.0)**2
205 V=(X7-0.0)**2 + (Y7-0.0)**2
206 V=(X8-0.0)**2 + (Y8-0.0)**2
207 V=(X9-0.0)**2 + (Y9-0.0)**2
208 V=(X10-0.0)**2 + (Y10-0.0)**2

```

```

209 V=(X1-0.0)**2 + (Y1-0.0)**2
210 V=(X2-0.0)**2 + (Y2-0.0)**2
211 V=(X3-0.0)**2 + (Y3-0.0)**2
212 V=(X4-0.0)**2 + (Y4-0.0)**2
213 V=(X5-0.0)**2 + (Y5-0.0)**2
214 V=(X6-0.0)**2 + (Y6-0.0)**2
215 V=(X7-0.0)**2 + (Y7-0.0)**2
216 V=(X8-0.0)**2 + (Y8-0.0)**2
217 V=(X9-0.0)**2 + (Y9-0.0)**2
218 V=(X10-0.0)**2 + (Y10-0.0)**2

```

```

219 V=(X1-0.0)**2 + (Y1-0.0)**2
220 V=(X2-0.0)**2 + (Y2-0.0)**2
221 V=(X3-0.0)**2 + (Y3-0.0)**2
222 V=(X4-0.0)**2 + (Y4-0.0)**2
223 V=(X5-0.0)**2 + (Y5-0.0)**2
224 V=(X6-0.0)**2 + (Y6-0.0)**2
225 V=(X7-0.0)**2 + (Y7-0.0)**2
226 V=(X8-0.0)**2 + (Y8-0.0)**2
227 V=(X9-0.0)**2 + (Y9-0.0)**2
228 V=(X10-0.0)**2 + (Y10-0.0)**2

```

```

229 V=(X1-0.0)**2 + (Y1-0.0)**2
230 V=(X2-0.0)**2 + (Y2-0.0)**2
231 V=(X3-0.0)**2 + (Y3-0.0)**2
232 V=(X4-0.0)**2 + (Y4-0.0)**2
233 V=(X5-0.0)**2 + (Y5-0.0)**2
234 V=(X6-0.0)**2 + (Y6-0.0)**2
235 V=(X7-0.0)**2 + (Y7-0.0)**2
236 V=(X8-0.0)**2 + (Y8-0.0)**2
237 V=(X9-0.0)**2 + (Y9-0.0)**2
238 V=(X10-0.0)**2 + (Y10-0.0)**2

```


1 SUBROUTINE INPUT: (DATA1, OF1, OF2, V1, S, I, MAX, CL, X, C, NY)
 2 DIMENSION DATA1(10, N), S(12), I MAX(3)
 3 COMPLEX DATA

4 FOR I=1, NY, NY, NY, NY
 5 DO 10 J=1, N
 6 READ (UNIT, I) DATA1(I, J), S(1), S(2), S(3), S(4), S(5), S(6), S(7), S(8), S(9), S(10), S(11), S(12), I MAX(I)

7 DO 10 J=1, N
 8 DO 10 K=1, NY

9 DO 10 L=1, NY
 10 DO 10 M=1, NY
 11 DO 10 N=1, NY
 12 DO 10 O=1, NY
 13 DO 10 P=1, NY
 14 DO 10 Q=1, NY
 15 DO 10 R=1, NY
 16 DO 10 S=1, NY
 17 DO 10 T=1, NY
 18 DO 10 U=1, NY
 19 DO 10 V=1, NY
 20 DO 10 W=1, NY
 21 DO 10 X=1, NY
 22 DO 10 Y=1, NY
 23 DO 10 Z=1, NY

24 DO 10 A=1, NY
 25 DO 10 B=1, NY
 26 DO 10 C=1, NY
 27 DO 10 D=1, NY
 28 DO 10 E=1, NY
 29 DO 10 F=1, NY
 30 DO 10 G=1, NY
 31 DO 10 H=1, NY
 32 DO 10 I=1, NY
 33 DO 10 J=1, NY
 34 DO 10 K=1, NY
 35 DO 10 L=1, NY
 36 DO 10 M=1, NY
 37 DO 10 N=1, NY
 38 DO 10 O=1, NY
 39 DO 10 P=1, NY
 40 DO 10 Q=1, NY
 41 DO 10 R=1, NY
 42 DO 10 S=1, NY
 43 DO 10 T=1, NY
 44 DO 10 U=1, NY
 45 DO 10 V=1, NY
 46 DO 10 W=1, NY
 47 DO 10 X=1, NY
 48 DO 10 Y=1, NY
 49 DO 10 Z=1, NY

```

5  A/32*W5+EXY
6  W/5*WNY + X-EXY
7  W/5*WNY + Y-EXY
8  CONTINUE
9  CONTINUE
10 W/5=AVG1 + AVG
11 W/5*(J)=W/5/2.0
12 CONTINUE
13 CONTINUE
14 COMPUTATION OF CENTROID
15 C=XE*W/5X/W/51
16 C=YE*W/5Y/W/52
17 CHECK FOR NO USAGE
18 VE
19 DO 3 J=1,N
20 IT(OUTAB(I),J)=LE-1.0E-6) K=K + 1
21 CONTINUE
22 IF (MULTIPLY) GO TO 23
23 STOP "TARGET HAS BEEN DRIVEN FROM PIYE- ARJAY."
24 PRINT "WILL GO TO NEXT PAGE OF DATA."
25 GOTO 26
26 STOP

```

SYMBOLIC REFERENCE MAP (S=2)

ENTRY POINTS

VARIABLES	SN	TYPE	DECLARATION
312	16G1	REAL	
314	16G2	REAL	
272	16G3	REAL	
315	16G4	REAL	
316	16G5	REAL	
277	16G6	REAL	
278	16G7	REAL	
317	16G8	REAL	
318	16G9	REAL	
279	16G10	REAL	
319	16G11	REAL	
280	16G12	REAL	
320	16G13	REAL	
281	16G14	REAL	
321	16G15	REAL	
282	16G16	REAL	
322	16G17	REAL	
283	16G18	REAL	
323	16G19	REAL	
284	16G20	REAL	
324	16G21	REAL	
285	16G22	REAL	
325	16G23	REAL	
286	16G24	REAL	
326	16G25	REAL	
287	16G26	REAL	
327	16G27	REAL	
288	16G28	REAL	
328	16G29	REAL	
289	16G30	REAL	
329	16G31	REAL	
290	16G32	REAL	
330	16G33	REAL	
291	16G34	REAL	
331	16G35	REAL	
292	16G36	REAL	
332	16G37	REAL	
293	16G38	REAL	
333	16G39	REAL	
294	16G40	REAL	
334	16G41	REAL	
295	16G42	REAL	
335	16G43	REAL	
296	16G44	REAL	
336	16G45	REAL	
297	16G46	REAL	
337	16G47	REAL	
298	16G48	REAL	
338	16G49	REAL	
299	16G50	REAL	
339	16G51	REAL	
300	16G52	REAL	
340	16G53	REAL	
301	16G54	REAL	
341	16G55	REAL	
302	16G56	REAL	
342	16G57	REAL	
303	16G58	REAL	
343	16G59	REAL	
304	16G60	REAL	
344	16G61	REAL	
305	16G62	REAL	
345	16G63	REAL	
306	16G64	REAL	
346	16G65	REAL	
307	16G66	REAL	
347	16G67	REAL	
308	16G68	REAL	
348	16G69	REAL	
309	16G70	REAL	
349	16G71	REAL	
310	16G72	REAL	
350	16G73	REAL	
311	16G74	REAL	
351	16G75	REAL	
312	16G76	REAL	
352	16G77	REAL	
313	16G78	REAL	
353	16G79	REAL	
314	16G80	REAL	
354	16G81	REAL	
315	16G82	REAL	
355	16G83	REAL	
316	16G84	REAL	
356	16G85	REAL	
317	16G86	REAL	
357	16G87	REAL	
318	16G88	REAL	
358	16G89	REAL	
319	16G90	REAL	
359	16G91	REAL	
320	16G92	REAL	
360	16G93	REAL	
321	16G94	REAL	
361	16G95	REAL	
322	16G96	REAL	
362	16G97	REAL	
323	16G98	REAL	
363	16G99	REAL	
324	16G100	REAL	
364	16G101	REAL	
325	16G102	REAL	
365	16G103	REAL	
326	16G104	REAL	
366	16G105	REAL	
327	16G106	REAL	
367	16G107	REAL	
328	16G108	REAL	
368	16G109	REAL	
329	16G110	REAL	
369	16G111	REAL	
330	16G112	REAL	
370	16G113	REAL	
331	16G114	REAL	
371	16G115	REAL	
332	16G116	REAL	
372	16G117	REAL	
333	16G118	REAL	
373	16G119	REAL	
334	16G120	REAL	
374	16G121	REAL	
335	16G122	REAL	
375	16G123	REAL	
336	16G124	REAL	
376	16G125	REAL	
337	16G126	REAL	
377	16G127	REAL	
338	16G128	REAL	
378	16G129	REAL	
339	16G130	REAL	
379	16G131	REAL	
340	16G132	REAL	
380	16G133	REAL	
341	16G134	REAL	
381	16G135	REAL	
342	16G136	REAL	
382	16G137	REAL	
343	16G138	REAL	
383	16G139	REAL	
344	16G140	REAL	
384	16G141	REAL	
345	16G142	REAL	
385	16G143	REAL	
346	16G144	REAL	
386	16G145	REAL	
347	16G146	REAL	
387	16G147	REAL	
348	16G148	REAL	
388	16G149	REAL	
349	16G150	REAL	
389	16G151	REAL	
350	16G152	REAL	
390	16G153	REAL	
351	16G154	REAL	
391	16G155	REAL	
352	16G156	REAL	
392	16G157	REAL	
353	16G158	REAL	
393	16G159	REAL	
354	16G160	REAL	
394	16G161	REAL	
355	16G162	REAL	
395	16G163	REAL	
356	16G164	REAL	
396	16G165	REAL	
357	16G166	REAL	
397	16G167	REAL	
358	16G168	REAL	
398	16G169	REAL	
359	16G170	REAL	
399	16G171	REAL	
360	16G172	REAL	
400	16G173	REAL	
361	16G174	REAL	
401	16G175	REAL	
362	16G176	REAL	
402	16G177	REAL	
363	16G178	REAL	
403	16G179	REAL	
364	16G180	REAL	
404	16G181	REAL	
365	16G182	REAL	
405	16G183	REAL	
366	16G184	REAL	
406	16G185	REAL	
367	16G186	REAL	
407	16G187	REAL	
368	16G188	REAL	
408	16G189	REAL	
369	16G190	REAL	
409	16G191	REAL	
370	16G192	REAL	
410	16G193	REAL	
371	16G194	REAL	
411	16G195	REAL	
372	16G196	REAL	
412	16G197	REAL	
373	16G198	REAL	
413	16G199	REAL	
374	16G200	REAL	
414	16G201	REAL	
375	16G202	REAL	
415	16G203	REAL	
376	16G204	REAL	
416	16G205	REAL	
377	16G206	REAL	
417	16G207	REAL	
378	16G208	REAL	
418	16G209	REAL	
379	16G210	REAL	
419	16G211	REAL	
380	16G212	REAL	
420	16G213	REAL	
381	16G214	REAL	
421	16G215	REAL	
382	16G216	REAL	
422	16G217	REAL	
383	16G218	REAL	
423	16G219	REAL	
384	16G220	REAL	
424	16G221	REAL	
385	16G222	REAL	
425	16G223	REAL	
386	16G224	REAL	
426	16G225	REAL	
387	16G226	REAL	
427	16G227	REAL	
388	16G228	REAL	
428	16G229	REAL	
389	16G230	REAL	
429	16G231	REAL	
390	16G232	REAL	
430	16G233	REAL	
391	16G234	REAL	
431	16G235	REAL	
392	16G236	REAL	
432	16G237	REAL	
393	16G238	REAL	
433	16G239	REAL	
394	16G240	REAL	
434	16G241	REAL	
395	16G242	REAL	
435	16G243	REAL	
396	16G244	REAL	
436	16G245	REAL	
397	16G246	REAL	
437	16G247	REAL	
398	16G248	REAL	
438	16G249	REAL	
399	16G250	REAL	
439	16G251	REAL	
400	16G252	REAL	
440	16G253	REAL	
401	16G254	REAL	
441	16G255	REAL	
402	16G256	REAL	
442	16G257	REAL	
403	16G258	REAL	
443	16G259	REAL	
404	16G260	REAL	
444	16G261	REAL	
405	16G262	REAL	
445	16G263	REAL	
406	16G264	REAL	
446	16G265	REAL	
407	16G266	REAL	
447	16G267	REAL	
408	16G268	REAL	
448	16G269	REAL	
409	16G270	REAL	
449	16G271	REAL	
410	16G272	REAL	
450	16G273	REAL	
411	16G274	REAL	
451	16G275	REAL	
412	16G276	REAL	
452	16G277	REAL	
413	16G278	REAL	
453	16G279	REAL	
414	16G280	REAL	
454	16G281	REAL	
415	16G282	REAL	
455	16G283	REAL	
416	16G284	REAL	
456	16G285	REAL	
417	16G286	REAL	
457	16G287	REAL	
418	16G288	REAL	
458	16G289	REAL	
419	16G290	REAL	
459	16G291	REAL	
420	16G292	REAL	
460	16G293	REAL	
421	16G294	REAL	
461	16G295	REAL	
422	16G296	REAL	
462	16G297	REAL	
423	16G298	REAL	
463	16G299	REAL	
424	16G300	REAL	
464	16G301	REAL	
425	16G302	REAL	
465	16G303	REAL	
426	16G304	REAL	
466	16G305	REAL	
427	16G306	REAL	
467	16G307	REAL	
428	16G308	REAL	
468	16G309	REAL	
429	16G310	REAL	
469	16G311	REAL	
430	16G312	REAL	
470	16G313	REAL	
431	16G314	REAL	
471	16G315	REAL	
432	16G316	REAL	
472	16G317	REAL	
433	16G318	REAL	
473	16G319	REAL	
434	16G320	REAL	
474	16G321	REAL	
435	16G322	REAL	
475	16G323	REAL	
436	16G324	REAL	
476	16G325	REAL	
437	16G326	REAL	
477	16G327	REAL	
438	16G328	REAL	
478	16G329	REAL	
439	16G330	REAL	
479	16G331	REAL	
440	16G332	REAL	
480	16G333	REAL	
441	16G334	REAL	
481	16G335	REAL	
442	16G336	REAL	
482	16G337	REAL	
443	16G338	REAL	
483	16G339	REAL	
444	16G340	REAL	
484	16G341	REAL	
445	16G342	REAL	
485	16G343	REAL	
446	16G344	REAL	
486	16G345	REAL	
447	16G346	REAL	
487	16G347	REAL	
448	16G348	REAL	
488	16G349	REAL	
4			


```

1  SUBROUTINE NOISE(M,IA,IA,K,S,IV,PHIN)
2  DESTRUCTOR (PHI(2),C1),R(S,IV),V(S),W(S),FHI(6),G),W(IN(54)
3  DESTRUCTOR WPA(6))
4  COMPILE DATA
5  DATA
6  IF(C1.EC.1) GO TO 17
7  IF(C1.EC.1) GO TO 11
8  IF(C1.EC.2) GO TO 12
9  IF(C1.EC.3) GO TO 12
10 CALL WPA(6,3) GO TO 12
11 ADDITION OF SPATIAL NOISE TO INPUT MATRIX
12 GENERATION OF GAUSSIAN VECTOR W
13 CALL WGEN(W)
14 COMPOSITION OF VECTOR
15 DATA
16 DATA
17 DATA
18 DATA
19 CALL WBLUFF(W,L,M,IA,IA,IA,IA,IA,IA,IA,IA)
20 GO TO 21
21 ADDITION OF TEMPORAL OR TEMPORAL WITH SPATIAL NOISE TO INPUT
22 GENERATION OF GAUSSIAN VECTOR
23 CALL WGEN(W)
24 COMPOSITION OF VECTOR
25 DATA
26 DATA
27 CALL WBLUFF(W,L,M,IA,IA,IA,IA,IA,IA,IA,IA)
28 DESTRUCTOR (PHI(2),C1),R(S,IV),V(S),W(S),FHI(6),G),W(IN(54)
29 DESTRUCTOR WPA(6))
30 CALL WPA(6,3) GO TO 12
31 COMPILE
32 ADDITION OF V TO W
33 DATA
34 V(I)=W(I) + W(I)
35 COMPILE
36 ADDITION OF NOISE TO INPUT ARRAY
37 DATA
38 DATA
39 DATA
40 DATA(I+5,J+5) = DATA(I+5,J+5) + V(K)
41 CONTINUE
42 RETURN
43 END

```

Best Available Copy

SYMBOLIC REFERENCE MAP (R-1)


```

SUBROUTINE AMV(K1,CENY,CENY,K2,SMV)
  DIMENSION SMV(1, 20),X(5)
  SAV(K2,1)=X(1) + X1(3) +200.
  SAV(K2,2)=CENY
  SAV(K2,3)=X1(2) + X1(1) +2-1.
  SAV(K2,4)=CENY
  SAV(K2,5)=SAV(K2,1) - CENY
  SAV(K2,6)=SAV(K2,3) - CENY
  END

```

SYMBOLIC REFERENCE MAP (REF)

ENTRY PRINTS 3 ONLY

SYMBOL	SYMBOL TYPE	DECLARATION	DECLARATION
K1	INT-GEN	F.P.	F.P.
K2	INT-GEN	F.P.	F.P.
SMV	ARRAY	REAL	REAL
X	ARRAY	REAL	REAL
X1	ARRAY	REAL	REAL

STATISTICS

PROGRAM LENGTH 288 19

Best Available Copy

SUBROUTINE CHEK1(A,S,II)
DIMENSION Z(N,N), Z(1,0)

DO 10 I=1,N
DO 10 J=1,N
Z(I,J)=0
Z(I,0)=0
Z(0,J)=0
Z(0,0)=0

DO 10 I=1,N
DO 10 J=1,N
Z(I,J)=A(I,J)-RES/R(J,J)
GO TO 11

CALL CHEK1(A,S,II)
DO 10 I=1,N
DO 10 J=1,N
Z(I,J)=S(I,J)+Z(I,J)+RES

DO 10 I=1,N
DO 10 J=1,N
Z(I,J)=S(I,J)+Z(I,J)+RES
GO TO 11

DO 10 I=1,N
DO 10 J=1,N
Z(I,J)=S(I,J)+Z(I,J)+RES
GO TO 11

DO 10 I=1,N
DO 10 J=1,N
Z(I,J)=S(I,J)+Z(I,J)+RES
GO TO 11

SYMBOLIC REFERENCE MAP (P.1)

ENTRY POINTS
3 CHEK1

VARIABLES	SN	TYPE	DECLARATION
I	1	INTEGER	ARRAY F.P.
J	2	INTEGER	ARRAY F.P.
K	3	INTEGER	ARRAY F.P.
L	4	INTEGER	ARRAY F.P.
M	5	REAL	ARRAY F.P.

EXTERNALS
OPT
LIBRARY

STATEMENT LABELS
10
11
12
13
14
15
16
17
18
19
20
21
22
23
24
25
26
27
28
29
30
31
32
33
34
35
36
37
38
39
40
41
42
43
44
45
46
47
48
49
50
51
52
53
54
55
56
57
58
59
60
61
62
63
64
65
66
67
68
69
70
71
72
73
74
75
76
77
78
79
80
81
82
83
84
85
86
87
88
89
90
91
92
93
94
95
96
97
98
99
100

ROUTINE WRITE 7877 DOT=1 PHOMP

```

1 SUBROUTINE PMSIT (A, B, C, I, J, K, L, M, N)
2   DIMENSION A (100), B (100), C (100)
3   PRINT *, " "
4   DO 30 J=1, N
5     DO 40 I=1, M
6       C (I, J, K) = A (I, J) + B (I, J, K)
7     CONTINUE
8   PRINT *, " "
9   RETURN
10  END

```

SYMBOLIC REFERENCE MAP (SRM)

ENTRY POINTS
3 UNFILE

VARIABLES	SU	SY	ALLOCATION
3	3	3	ARRAY
20	10	10	F.P.
5	5	5	F.P.

FILE NAMES
79 OUTPUT

STATEMENT LABELS
47 140 141

LOOPS	LFEE	LINE	FLOW-TO	LENGTH	PROPERTIES
13	30	10	4	20	EXT REFS
10	10	10	5	10	EXT REFS

STATISTICS

PROGRAM LENGTH 600

Best Available Copy


```

CVR20 = FI-FY/CF2/DEM
VY=20LY( . , FYY)
N 17 I=1,21
FX=I-12
FX(22)=FI-FX/CF1/DEM
XC(20)LY( . , FXX)
MCA(20)=MCA(0,1) *CEXP(XX+YY)
CONTINUE
2000=SERIAL (USE TO HANDLE TOP OF 12TH HARMONIC BLOCK)
CX=1
FX(20)=FI-FY/CF1/DEM
XC(20)LY( . , FXX)
N 17 I=2,21
FX=I-12
FX(22)=FI-FX/CF1/DEM
VY=20LY( . , FYY)
MCA(20)=MCA(0,1) *CEXP(XX+YY)
CONTINUE
11
2001=SERIAL (USE TO HANDLE 3RD BACK INTO FOURTH FORMAT)
CX=1
MCA(20)=MCA(0,1) *CEXP(XX+YY)
CONTINUE
12
DATA(11,20)=MCA(1,12)
DATA(11,20)=MCA(1,12)
CONTINUE
SMITH CUSTOMER'S 1 AND 2
N 17 I=1,21
N 17 J=1,21
DATA(11,20)=MCA(1,12)
DATA(11,20)=MCA(1,12)
CONTINUE
13
DATA(11,20)=MCA(1,12)
DATA(11,20)=MCA(1,12)
CONTINUE
14
DATA(11,20)=MCA(1,12)
DATA(11,20)=MCA(1,12)
CONTINUE
15
DATA(11,20)=MCA(1,12)
DATA(11,20)=MCA(1,12)
CONTINUE
16
DATA(11,20)=MCA(1,12)
DATA(11,20)=MCA(1,12)
CONTINUE
17
DATA(11,20)=MCA(1,12)
DATA(11,20)=MCA(1,12)
CONTINUE
18
DATA(11,20)=MCA(1,12)
DATA(11,20)=MCA(1,12)
CONTINUE
19
DATA(11,20)=MCA(1,12)
DATA(11,20)=MCA(1,12)
CONTINUE
20
DATA(11,20)=MCA(1,12)
DATA(11,20)=MCA(1,12)
CONTINUE
21
DATA(11,20)=MCA(1,12)
DATA(11,20)=MCA(1,12)
CONTINUE
22
DATA(11,20)=MCA(1,12)
DATA(11,20)=MCA(1,12)
CONTINUE
23
DATA(11,20)=MCA(1,12)
DATA(11,20)=MCA(1,12)
CONTINUE
24
DATA(11,20)=MCA(1,12)
DATA(11,20)=MCA(1,12)
CONTINUE
25
DATA(11,20)=MCA(1,12)
DATA(11,20)=MCA(1,12)
CONTINUE
26
DATA(11,20)=MCA(1,12)
DATA(11,20)=MCA(1,12)
CONTINUE
27
DATA(11,20)=MCA(1,12)
DATA(11,20)=MCA(1,12)
CONTINUE
28
DATA(11,20)=MCA(1,12)
DATA(11,20)=MCA(1,12)
CONTINUE
29
DATA(11,20)=MCA(1,12)
DATA(11,20)=MCA(1,12)
CONTINUE
30
DATA(11,20)=MCA(1,12)
DATA(11,20)=MCA(1,12)
CONTINUE
31
DATA(11,20)=MCA(1,12)
DATA(11,20)=MCA(1,12)
CONTINUE
32
DATA(11,20)=MCA(1,12)
DATA(11,20)=MCA(1,12)
CONTINUE
33
DATA(11,20)=MCA(1,12)
DATA(11,20)=MCA(1,12)
CONTINUE
34
DATA(11,20)=MCA(1,12)
DATA(11,20)=MCA(1,12)
CONTINUE
35
DATA(11,20)=MCA(1,12)
DATA(11,20)=MCA(1,12)
CONTINUE
36
DATA(11,20)=MCA(1,12)
DATA(11,20)=MCA(1,12)
CONTINUE
37
DATA(11,20)=MCA(1,12)
DATA(11,20)=MCA(1,12)
CONTINUE
38
DATA(11,20)=MCA(1,12)
DATA(11,20)=MCA(1,12)
CONTINUE
39
DATA(11,20)=MCA(1,12)
DATA(11,20)=MCA(1,12)
CONTINUE
40
DATA(11,20)=MCA(1,12)
DATA(11,20)=MCA(1,12)
CONTINUE
41
DATA(11,20)=MCA(1,12)
DATA(11,20)=MCA(1,12)
CONTINUE
42
DATA(11,20)=MCA(1,12)
DATA(11,20)=MCA(1,12)
CONTINUE
43
DATA(11,20)=MCA(1,12)
DATA(11,20)=MCA(1,12)
CONTINUE
44
DATA(11,20)=MCA(1,12)
DATA(11,20)=MCA(1,12)
CONTINUE
45
DATA(11,20)=MCA(1,12)
DATA(11,20)=MCA(1,12)
CONTINUE
46
DATA(11,20)=MCA(1,12)
DATA(11,20)=MCA(1,12)
CONTINUE
47
DATA(11,20)=MCA(1,12)
DATA(11,20)=MCA(1,12)
CONTINUE
48
DATA(11,20)=MCA(1,12)
DATA(11,20)=MCA(1,12)
CONTINUE
49
DATA(11,20)=MCA(1,12)
DATA(11,20)=MCA(1,12)
CONTINUE
50
DATA(11,20)=MCA(1,12)
DATA(11,20)=MCA(1,12)
CONTINUE
51
DATA(11,20)=MCA(1,12)
DATA(11,20)=MCA(1,12)
CONTINUE
52
DATA(11,20)=MCA(1,12)
DATA(11,20)=MCA(1,12)
CONTINUE
53
DATA(11,20)=MCA(1,12)
DATA(11,20)=MCA(1,12)
CONTINUE
54
DATA(11,20)=MCA(1,12)
DATA(11,20)=MCA(1,12)
CONTINUE
55
DATA(11,20)=MCA(1,12)
DATA(11,20)=MCA(1,12)
CONTINUE
56
DATA(11,20)=MCA(1,12)
DATA(11,20)=MCA(1,12)
CONTINUE
57
DATA(11,20)=MCA(1,12)
DATA(11,20)=MCA(1,12)
CONTINUE
58
DATA(11,20)=MCA(1,12)
DATA(11,20)=MCA(1,12)
CONTINUE
59
DATA(11,20)=MCA(1,12)
DATA(11,20)=MCA(1,12)
CONTINUE
60
DATA(11,20)=MCA(1,12)
DATA(11,20)=MCA(1,12)
CONTINUE
61
DATA(11,20)=MCA(1,12)
DATA(11,20)=MCA(1,12)
CONTINUE
62
DATA(11,20)=MCA(1,12)
DATA(11,20)=MCA(1,12)
CONTINUE
63
DATA(11,20)=MCA(1,12)
DATA(11,20)=MCA(1,12)
CONTINUE
64
DATA(11,20)=MCA(1,12)
DATA(11,20)=MCA(1,12)
CONTINUE
65
DATA(11,20)=MCA(1,12)
DATA(11,20)=MCA(1,12)
CONTINUE
66
DATA(11,20)=MCA(1,12)
DATA(11,20)=MCA(1,12)
CONTINUE
67
DATA(11,20)=MCA(1,12)
DATA(11,20)=MCA(1,12)
CONTINUE
68
DATA(11,20)=MCA(1,12)
DATA(11,20)=MCA(1,12)
CONTINUE
69
DATA(11,20)=MCA(1,12)
DATA(11,20)=MCA(1,12)
CONTINUE
70
DATA(11,20)=MCA(1,12)
DATA(11,20)=MCA(1,12)
CONTINUE
71
DATA(11,20)=MCA(1,12)
DATA(11,20)=MCA(1,12)
CONTINUE
72
DATA(11,20)=MCA(1,12)
DATA(11,20)=MCA(1,12)
CONTINUE
73
DATA(11,20)=MCA(1,12)
DATA(11,20)=MCA(1,12)
CONTINUE
74
DATA(11,20)=MCA(1,12)
DATA(11,20)=MCA(1,12)
CONTINUE
75
DATA(11,20)=MCA(1,12)
DATA(11,20)=MCA(1,12)
CONTINUE
76
DATA(11,20)=MCA(1,12)
DATA(11,20)=MCA(1,12)
CONTINUE
77
DATA(11,20)=MCA(1,12)
DATA(11,20)=MCA(1,12)
CONTINUE
78
DATA(11,20)=MCA(1,12)
DATA(11,20)=MCA(1,12)
CONTINUE
79
DATA(11,20)=MCA(1,12)
DATA(11,20)=MCA(1,12)
CONTINUE
80
DATA(11,20)=MCA(1,12)
DATA(11,20)=MCA(1,12)
CONTINUE
81
DATA(11,20)=MCA(1,12)
DATA(11,20)=MCA(1,12)
CONTINUE
82
DATA(11,20)=MCA(1,12)
DATA(11,20)=MCA(1,12)
CONTINUE
83
DATA(11,20)=MCA(1,12)
DATA(11,20)=MCA(1,12)
CONTINUE
84
DATA(11,20)=MCA(1,12)
DATA(11,20)=MCA(1,12)
CONTINUE
85
DATA(11,20)=MCA(1,12)
DATA(11,20)=MCA(1,12)
CONTINUE
86
DATA(11,20)=MCA(1,12)
DATA(11,20)=MCA(1,12)
CONTINUE
87
DATA(11,20)=MCA(1,12)
DATA(11,20)=MCA(1,12)
CONTINUE
88
DATA(11,20)=MCA(1,12)
DATA(11,20)=MCA(1,12)
CONTINUE
89
DATA(11,20)=MCA(1,12)
DATA(11,20)=MCA(1,12)
CONTINUE
90
DATA(11,20)=MCA(1,12)
DATA(11,20)=MCA(1,12)
CONTINUE
91
DATA(11,20)=MCA(1,12)
DATA(11,20)=MCA(1,12)
CONTINUE
92
DATA(11,20)=MCA(1,12)
DATA(11,20)=MCA(1,12)
CONTINUE
93
DATA(11,20)=MCA(1,12)
DATA(11,20)=MCA(1,12)
CONTINUE
94
DATA(11,20)=MCA(1,12)
DATA(11,20)=MCA(1,12)
CONTINUE
95
DATA(11,20)=MCA(1,12)
DATA(11,20)=MCA(1,12)
CONTINUE
96
DATA(11,20)=MCA(1,12)
DATA(11,20)=MCA(1,12)
CONTINUE
97
DATA(11,20)=MCA(1,12)
DATA(11,20)=MCA(1,12)
CONTINUE
98
DATA(11,20)=MCA(1,12)
DATA(11,20)=MCA(1,12)
CONTINUE
99
DATA(11,20)=MCA(1,12)
DATA(11,20)=MCA(1,12)
CONTINUE
100
DATA(11,20)=MCA(1,12)
DATA(11,20)=MCA(1,12)
CONTINUE

```

SYMBOLS REFERENCE MAP (REV)

ENTRY POINTS
3 SHIFT

VARIABLES	SN	TYPE	ALLOCATION	UNIT	LOC.
355	FX	REAL	355	DEH	REAL
371	FX1	REAL	371	FX1	REAL
376	FX1	REAL	376	FX2	REAL
376	FX1	REAL	377	FX2	REAL
382	FY1	REAL	383	FY1	REAL
382	FY1	REAL	381	FY2	REAL
384	I1	INTEGER	384	I1	INTEGER
384	I1	INTEGER	385	I2	INTEGER
381	J1	INTEGER	385	J1	INTEGER
373	J1	INTEGER	384	J2	INTEGER
376	J1	INTEGER	377	J2	INTEGER
376	J1	REAL	377	J2	REAL

Best Available Copy


```

37 CONTINUE
   DO 3, I=1,N
   LEIS=
   DO 3, J=1,N
   IF (A(I,J) .EQ. 0) GO TO 35
   CALL CHOL(1,1,1)
   DO 3, I=1,N
   DO 3, J=1,N
   CALL CHOL(1,1,1)
   CONTINUE
   PRINT 11
   F=1.0/((1.0/2.0)*N*(N+1.0))
   CALL WDATE (1973,12,27)
   COMPUTE THE CHOLESKY SQUARE ROOT OF RN
   CALL CHOL(1,1,1)
   PRINT 12
   F=1.0/((1.0/2.0)*N*(N+1.0))
   CALL WDATE (1973,12,27)
   END

```

SYMBOLIC REFERENCING AND (F=1)

ENTRY POINTS
3 SPIN

VARIABLES	SM	TYPE	RELOCATION	ARRAY	F.P.
202 J	1	INTEGER			
201 I	1	INTEGER			
200 N	1	INTEGER			
199 N	1	REAL			
198 N	1	SIGMA			
FILE NAMES		MODE			
OUTPUT		FILE			

EXTENS	CHSKI	TYPE	SEGS
201 I		ARRAY	F.P.
202 J		ARRAY	F.P.
200 N		ARRAY	F.P.
199 N		REAL	F.P.

STATEMENT LABELS	LOCUS	LINE	LEN	CH	TYPE	SEGS
117 38	117	38	1	I	IF	173
176 27	176	27	1	I	IF	173
132 26	132	26	1	I	IF	173
106 25	106	25	1	I	IF	173
227 18	227	18	1	I	IF	173
173 34	173	34	1	I	IF	173
173 34	173	34	1	I	IF	173

LOCUS	LINE	LEN	CH	TYPE	SEGS
117 38	117	38	1	I	IF
176 27	176	27	1	I	IF
132 26	132	26	1	I	IF
106 25	106	25	1	I	IF
227 18	227	18	1	I	IF
173 34	173	34	1	I	IF
173 34	173	34	1	I	IF

Best Available Copy 84

```

1 SUBROUTINE HSB(Z,RLH,LH,XH,P,ALIM,XP,FP)
  C=1/ST(7(1)),LH(1),LH(2),LH(3),LH(4)
  1 YD(1),YD(2),YD(3),YD(4),PP(1),PP(2),PP(3),PP(4),RTH(1),RTH(2),RTH(3),RTH(4)
  2 XMA(1),XMA(2),XMA(3),XMA(4),R(1),R(2),R(3),R(4)
  3 REAL RLH,LH,LH,XP,FP
  4 *** COMPUTATION OF COVARIANCE PLUS MATRIX USING INVERSE COVARIANCE FORM ***
  5 DO 10 I=1,4
    DO 10 J=1,4
      LPT(I,J)=LH(I)*LH(J)
  10 CONTINUE
  11 L=1
  12 DO 20 I=1,4
    DO 20 J=1,4
      L=L+1
      CALL VMLUFF(LPT,LH,LH,N,I,J,3,HI,I,DI,IER)
      I=I+1
  20 CONTINUE
  21 CALL LIRZF(FP,M,IA,PIRV,IOSI,ANKS,IER)
  22 S=1
  23 DO 30 I=1,4
    DO 30 J=1,4
      S=S+1
      FLM(I,J)=FPM(I,J)+RINV*HTH(I,J)
  30 CONTINUE
  31 DO 40 I=1,4
    DO 40 J=1,4
      CALL LIRZF(PIV,M,IA,PI,IOSI,ANKS,IER)
      S=I+1
      S=J+1
      S=S+1
      S=S+1
  40 CONTINUE
  41 CALL VMLUFF(FP,LH(LH,N,I,3),K,I,DI,IER)
  42 DO 50 I=1,4
    DO 50 J=1,4
      FLM(I,J)=FLM(I,J)+PIV
  50 CONTINUE
  51 *** COMPUTATION OF KALMAN FILTER GAIN ***
  52 L=1
  53 DO 60 I=1,4
    DO 60 J=1,4
      L=L+1
      CALL VMLUFF(FP,LH(LH,N,I,3),K,I,DI,IER)
  60 CONTINUE
  61 DO 70 I=1,4
    DO 70 J=1,4
      L=L+1
      CALL VMLUFF(FP,LH(LH,N,I,3),K,I,DI,IER)
  70 CONTINUE
  71 *** COMPUTATION OF STATE MEASUREMENT UPDATE ***
  72 DO 80 I=1,4
    DO 80 J=1,4
      L=L+1
      CALL VMLUFF(FP,LH(LH,N,I,3),K,I,DI,IER)
  80 CONTINUE
  81 DO 90 I=1,4
    DO 90 J=1,4
      L=L+1
      CALL VMLUFF(FP,LH(LH,N,I,3),K,I,DI,IER)
  90 CONTINUE
  91 DO 100 I=1,4
    DO 100 J=1,4
      L=L+1
      CALL VMLUFF(FP,LH(LH,N,I,3),K,I,DI,IER)
  100 CONTINUE

```



```

1  SUBROUTINE VEC(N,M)
   OF (VECTOR) M(R)
   DO 10 J=1,M
   10  TOTAL = 0
   DO 20 I=1,N
   20  TOTAL = TOTAL + A(I,J)
   30  CONTINUE
   M(TOTAL) = TOTAL
   RETURN
   END

```

SYMBOLIC REFERENCE MAP (SRI)

ENTRY POINTS
3 VEC

VARIABLES	SR	TYPE	ADDRESS	ALLOCATION
1. J		REAL		
2. I		INTEGER		
27 TOTAL		REAL		

NO	I	INTEGER	REAL	ARRAY	S.P.	F.P.
1	1					
2	1					
3	1					

87 INCLUDE FUNCTIONS TYPE ADDR
REAL 1 INTFR

STATEMENT LABELS

0 10

LOOPS	LABEL	ENTRY	EXIT	LENGTH	PROPERTIES
1	10	J	3	104	NOT INVED
2	20	I	5	53	INSTACK

STATISTICS
PROGRAM LENGTH 304 25
PROGRAM DO 21 USED

Best Available Copy

SUBROUTINE FOURIER TRANSFORM IN USASI BASIC FUNCTION
FOR INFORMATION CONTACT DR. MARK ALLER 431 7400S/50259

14. COOLY-TIMMY FAST FOURIER TRANSFORM IN USASI BASIC FUNCTION

```

      TRNDFD(1:4) = 0.0
      TRNDFD(5:8) = 0.0
      TRNDFD(9:12) = 0.0
      TRNDFD(13:16) = 0.0
      TRNDFD(17:20) = 0.0
      TRNDFD(21:24) = 0.0
      TRNDFD(25:28) = 0.0
      TRNDFD(29:32) = 0.0
      TRNDFD(33:36) = 0.0
      TRNDFD(37:40) = 0.0
      TRNDFD(41:44) = 0.0
      TRNDFD(45:48) = 0.0
      TRNDFD(49:52) = 0.0
      TRNDFD(53:56) = 0.0
      TRNDFD(57:60) = 0.0
      TRNDFD(61:64) = 0.0
      TRNDFD(65:68) = 0.0
      TRNDFD(69:72) = 0.0
      TRNDFD(73:76) = 0.0
      TRNDFD(77:80) = 0.0
      TRNDFD(81:84) = 0.0
      TRNDFD(85:88) = 0.0
      TRNDFD(89:92) = 0.0
      TRNDFD(93:96) = 0.0
      TRNDFD(97:100) = 0.0
      TRNDFD(101:104) = 0.0
      TRNDFD(105:108) = 0.0
      TRNDFD(109:112) = 0.0
      TRNDFD(113:116) = 0.0
      TRNDFD(117:120) = 0.0
      TRNDFD(121:124) = 0.0
      TRNDFD(125:128) = 0.0
      TRNDFD(129:132) = 0.0
      TRNDFD(133:136) = 0.0
      TRNDFD(137:140) = 0.0
      TRNDFD(141:144) = 0.0
      TRNDFD(145:148) = 0.0
      TRNDFD(149:152) = 0.0
      TRNDFD(153:156) = 0.0
      TRNDFD(157:160) = 0.0
      TRNDFD(161:164) = 0.0
      TRNDFD(165:168) = 0.0
      TRNDFD(169:172) = 0.0
      TRNDFD(173:176) = 0.0
      TRNDFD(177:180) = 0.0
      TRNDFD(181:184) = 0.0
      TRNDFD(185:188) = 0.0
      TRNDFD(189:192) = 0.0
      TRNDFD(193:196) = 0.0
      TRNDFD(197:200) = 0.0
      TRNDFD(201:204) = 0.0
      TRNDFD(205:208) = 0.0
      TRNDFD(209:212) = 0.0
      TRNDFD(213:216) = 0.0
      TRNDFD(217:220) = 0.0
      TRNDFD(221:224) = 0.0
      TRNDFD(225:228) = 0.0
      TRNDFD(229:232) = 0.0
      TRNDFD(233:236) = 0.0
      TRNDFD(237:240) = 0.0
      TRNDFD(241:244) = 0.0
      TRNDFD(245:248) = 0.0
      TRNDFD(249:252) = 0.0
      TRNDFD(253:256) = 0.0
      TRNDFD(257:260) = 0.0
      TRNDFD(261:264) = 0.0
      TRNDFD(265:268) = 0.0
      TRNDFD(269:272) = 0.0
      TRNDFD(273:276) = 0.0
      TRNDFD(277:280) = 0.0
      TRNDFD(281:284) = 0.0
      TRNDFD(285:288) = 0.0
      TRNDFD(289:292) = 0.0
      TRNDFD(293:296) = 0.0
      TRNDFD(297:300) = 0.0
      TRNDFD(301:304) = 0.0
      TRNDFD(305:308) = 0.0
      TRNDFD(309:312) = 0.0
      TRNDFD(313:316) = 0.0
      TRNDFD(317:320) = 0.0
      TRNDFD(321:324) = 0.0
      TRNDFD(325:328) = 0.0
      TRNDFD(329:332) = 0.0
      TRNDFD(333:336) = 0.0
      TRNDFD(337:340) = 0.0
      TRNDFD(341:344) = 0.0
      TRNDFD(345:348) = 0.0
      TRNDFD(349:352) = 0.0
      TRNDFD(353:356) = 0.0
      TRNDFD(357:360) = 0.0
      TRNDFD(361:364) = 0.0
      TRNDFD(365:368) = 0.0
      TRNDFD(369:372) = 0.0
      TRNDFD(373:376) = 0.0
      TRNDFD(377:380) = 0.0
      TRNDFD(381:384) = 0.0
      TRNDFD(385:388) = 0.0
      TRNDFD(389:392) = 0.0
      TRNDFD(393:396) = 0.0
      TRNDFD(397:400) = 0.0
      TRNDFD(401:404) = 0.0
      TRNDFD(405:408) = 0.0
      TRNDFD(409:412) = 0.0
      TRNDFD(413:416) = 0.0
      TRNDFD(417:420) = 0.0
      TRNDFD(421:424) = 0.0
      TRNDFD(425:428) = 0.0
      TRNDFD(429:432) = 0.0
      TRNDFD(433:436) = 0.0
      TRNDFD(437:440) = 0.0
      TRNDFD(441:444) = 0.0
      TRNDFD(445:448) = 0.0
      TRNDFD(449:452) = 0.0
      TRNDFD(453:456) = 0.0
      TRNDFD(457:460) = 0.0
      TRNDFD(461:464) = 0.0
      TRNDFD(465:468) = 0.0
      TRNDFD(469:472) = 0.0
      TRNDFD(473:476) = 0.0
      TRNDFD(477:480) = 0.0
      TRNDFD(481:484) = 0.0
      TRNDFD(485:488) = 0.0
      TRNDFD(489:492) = 0.0
      TRNDFD(493:496) = 0.0
      TRNDFD(497:500) = 0.0
      TRNDFD(501:504) = 0.0
      TRNDFD(505:508) = 0.0
      TRNDFD(509:512) = 0.0
      TRNDFD(513:516) = 0.0
      TRNDFD(517:520) = 0.0
      TRNDFD(521:524) = 0.0
      TRNDFD(525:528) = 0.0
      TRNDFD(529:532) = 0.0
      TRNDFD(533:536) = 0.0
      TRNDFD(537:540) = 0.0
      TRNDFD(541:544) = 0.0
      TRNDFD(545:548) = 0.0
      TRNDFD(549:552) = 0.0
      TRNDFD(553:556) = 0.0
      TRNDFD(557:560) = 0.0
      TRNDFD(561:564) = 0.0
      TRNDFD(565:568) = 0.0
      TRNDFD(569:572) = 0.0
      TRNDFD(573:576) = 0.0
      TRNDFD(577:580) = 0.0
      TRNDFD(581:584) = 0.0
      TRNDFD(585:588) = 0.0
      TRNDFD(589:592) = 0.0
      TRNDFD(593:596) = 0.0
      TRNDFD(597:600) = 0.0
      TRNDFD(601:604) = 0.0
      TRNDFD(605:608) = 0.0
      TRNDFD(609:612) = 0.0
      TRNDFD(613:616) = 0.0
      TRNDFD(617:620) = 0.0
      TRNDFD(621:624) = 0.0
      TRNDFD(625:628) = 0.0
      TRNDFD(629:632) = 0.0
      TRNDFD(633:636) = 0.0
      TRNDFD(637:640) = 0.0
      TRNDFD(641:644) = 0.0
      TRNDFD(645:648) = 0.0
      TRNDFD(649:652) = 0.0
      TRNDFD(653:656) = 0.0
      TRNDFD(657:660) = 0.0
      TRNDFD(661:664) = 0.0
      TRNDFD(665:668) = 0.0
      TRNDFD(669:672) = 0.0
      TRNDFD(673:676) = 0.0
      TRNDFD(677:680) = 0.0
      TRNDFD(681:684) = 0.0
      TRNDFD(685:688) = 0.0
      TRNDFD(689:692) = 0.0
      TRNDFD(693:696) = 0.0
      TRNDFD(697:700) = 0.0
      TRNDFD(701:704) = 0.0
      TRNDFD(705:708) = 0.0
      TRNDFD(709:712) = 0.0
      TRNDFD(713:716) = 0.0
      TRNDFD(717:720) = 0.0
      TRNDFD(721:724) = 0.0
      TRNDFD(725:728) = 0.0
      TRNDFD(729:732) = 0.0
      TRNDFD(733:736) = 0.0
      TRNDFD(737:740) = 0.0
      TRNDFD(741:744) = 0.0
      TRNDFD(745:748) = 0.0
      TRNDFD(749:752) = 0.0
      TRNDFD(753:756) = 0.0
      TRNDFD(757:760) = 0.0
      TRNDFD(761:764) = 0.0
      TRNDFD(765:768) = 0.0
      TRNDFD(769:772) = 0.0
      TRNDFD(773:776) = 0.0
      TRNDFD(777:780) = 0.0
      TRNDFD(781:784) = 0.0
      TRNDFD(785:788) = 0.0
      TRNDFD(789:792) = 0.0
      TRNDFD(793:796) = 0.0
      TRNDFD(797:800) = 0.0
      TRNDFD(801:804) = 0.0
      TRNDFD(805:808) = 0.0
      TRNDFD(809:812) = 0.0
      TRNDFD(813:816) = 0.0
      TRNDFD(817:820) = 0.0
      TRNDFD(821:824) = 0.0
      TRNDFD(825:828) = 0.0
      TRNDFD(829:832) = 0.0
      TRNDFD(833:836) = 0.0
      TRNDFD(837:840) = 0.0
      TRNDFD(841:844) = 0.0
      TRNDFD(845:848) = 0.0
      TRNDFD(849:852) = 0.0
      TRNDFD(853:856) = 0.0
      TRNDFD(857:860) = 0.0
      TRNDFD(861:864) = 0.0
      TRNDFD(865:868) = 0.0
      TRNDFD(869:872) = 0.0
      TRNDFD(873:876) = 0.0
      TRNDFD(877:880) = 0.0
      TRNDFD(881:884) = 0.0
      TRNDFD(885:888) = 0.0
      TRNDFD(889:892) = 0.0
      TRNDFD(893:896) = 0.0
      TRNDFD(897:900) = 0.0
      TRNDFD(901:904) = 0.0
      TRNDFD(905:908) = 0.0
      TRNDFD(909:912) = 0.0
      TRNDFD(913:916) = 0.0
      TRNDFD(917:920) = 0.0
      TRNDFD(921:924) = 0.0
      TRNDFD(925:928) = 0.0
      TRNDFD(929:932) = 0.0
      TRNDFD(933:936) = 0.0
      TRNDFD(937:940) = 0.0
      TRNDFD(941:944) = 0.0
      TRNDFD(945:948) = 0.0
      TRNDFD(949:952) = 0.0
      TRNDFD(953:956) = 0.0
      TRNDFD(957:960) = 0.0
      TRNDFD(961:964) = 0.0
      TRNDFD(965:968) = 0.0
      TRNDFD(969:972) = 0.0
      TRNDFD(973:976) = 0.0
      TRNDFD(977:980) = 0.0
      TRNDFD(981:984) = 0.0
      TRNDFD(985:988) = 0.0
      TRNDFD(989:992) = 0.0
      TRNDFD(993:996) = 0.0
      TRNDFD(997:1000) = 0.0

```

1. THE NUMBER OF INPUT DATA AND THE NUMBER OF TRANSFORM VALUES
 2. BOTH THE INPUT DATA AND THE TRANSFORM VALUES MUST REPRESENT
 EQUIVALENT POINTS IN THEIR RESPECTIVE DOMAINS OF TIME AND
 FREQUENCY. CALLING THESE SPACINGS DELTA1 AND DELTA2, IT MUST BE
 TRUE THAT DELTA1/DELTA2 = PI/(MCI*DELTA1). OF COURSE, DELTA1 NEED NOT
 BE THE SAME FOR EVERY DIMENSION.

PROGRAM BY TOMMY RECHNER FROM THE BASIC PROGRAM BY CHARLES
 RABIN. WALTER POLY SUGGESTED THE IDEA FOR THE DIGIT SEVERAL.
 THE SMALL LETTERS, SUBJECT LINE. THIS IS THE FASTEST AND MOST
 VERSATILE VERSION OF THE FFT KNOWN TO THE AUTHOR. SHOULD BE
 GOOD FOR ALL FOURIER TRANSFORM DIMENSION LENGTHS TO COVER OF TWO.
 SEVERAL AURAL TRANSACTIONS (JUNE 1967), SPECIAL ISSUE IN FFT.


```

115 3' 1003=I/IDIV
116 3' 104=I/IDIV
117 31 IF(COUNT-IDIV) 10,31,31
118 32 IF(LCEN) 10,32,31
119 33 IFACT(IIF)=I/IDIV
120 34 107=IDIV+2
121 35 GO TO 3
122 36 IF(LCEN) 10,36,31
123 37 1000=IDIV+1
124 38 GO TO 3
125 39 IFACT(IIF)=I
126 40 SEPARATE FIVE CASES--
127 41 1. COMPLEX TRANSFORM OR REAL TRANSFORM FOR THE 4TH, 5TH, ETC.
128 42 OPERATIONS.
129 43 2. REAL TRANSFORM FOR THE 2ND OR 3RD DIMENSION. METHOD--
130 44 TRANSFORM HALF THE DATA, SUPPLYING THE OTHER HALF BY CON-
131 45 JUGATE SYMMETRY.
132 46 3. REAL TRANSFORM FOR THE 1ST DIMENSION. N ODL. METHOD--
133 47 TRANSFORM HALF THE DATA AT EACH STAGE, SUPPLYING THE OTHER
134 48 HALF BY CONJUGATE SYMMETRY.
135 49 4. REAL TRANSFORM FOR THE 1ST DIMENSION, K EVEN. METHOD--
136 50 TRANSFORM COMPLEX ARRAY OF LENGTH N/2 WHOSE REAL PARTS
137 51 ARE THE EVEN-NUMBERED REAL VALUES AND WHOSE IMAGINARY PARTS
138 52 ARE THE ODD-NUMBERED REAL VALUES. SEPARATE AND SUPPLY
139 53 THE SECOND HALF BY CONJUGATE SYMMETRY.
140 54 1002=ID1*(N/2+1)
141 55 1003=I
142 56 IF(IPT=1) 1003,1
143 57 1000=ID1*(N/2+1)
144 58 1003=I
145 59 1000=ID1*(N/2+1)
146 60 1003=I
147 61 1000=ID1*(N/2+1)
148 62 1003=I
149 63 1000=ID1*(N/2+1)
150 64 1003=I
151 65 DATA(1)=DATA(1)
152 66 I=I+2
153 67 I=I+2
154 68 IF(I=I) 1003,1
155 69 1000=ID1*(N/2+1)
156 70 1003=I
157 71 1000=ID1*(N/2+1)
158 72 1003=I
159 73 1000=ID1*(N/2+1)
160 74 1003=I
161 75 1000=ID1*(N/2+1)
162 76 1003=I
163 77 1000=ID1*(N/2+1)
164 78 1003=I
165 79 1000=ID1*(N/2+1)
166 80 1003=I
167 81 1000=ID1*(N/2+1)
168 82 1003=I
169 83 1000=ID1*(N/2+1)
170 84 1003=I
171 85 1000=ID1*(N/2+1)
172 86 1003=I
173 87 1000=ID1*(N/2+1)
174 88 1003=I
175 89 1000=ID1*(N/2+1)
176 90 1003=I
177 91 1000=ID1*(N/2+1)
178 92 1003=I
179 93 1000=ID1*(N/2+1)
180 94 1003=I
181 95 1000=ID1*(N/2+1)
182 96 1003=I
183 97 1000=ID1*(N/2+1)
184 98 1003=I
185 99 1000=ID1*(N/2+1)
186 100 1003=I
187 101 1000=ID1*(N/2+1)
188 102 1003=I
189 103 1000=ID1*(N/2+1)
190 104 1003=I
191 105 1000=ID1*(N/2+1)
192 106 1003=I
193 107 1000=ID1*(N/2+1)
194 108 1003=I
195 109 1000=ID1*(N/2+1)
196 110 1003=I
197 111 1000=ID1*(N/2+1)
198 112 1003=I
199 113 1000=ID1*(N/2+1)
200 114 1003=I
201 115 1000=ID1*(N/2+1)
202 116 1003=I
203 117 1000=ID1*(N/2+1)
204 118 1003=I
205 119 1000=ID1*(N/2+1)
206 120 1003=I
207 121 1000=ID1*(N/2+1)
208 122 1003=I
209 123 1000=ID1*(N/2+1)
210 124 1003=I
211 125 1000=ID1*(N/2+1)
212 126 1003=I
213 127 1000=ID1*(N/2+1)
214 128 1003=I
215 129 1000=ID1*(N/2+1)
216 130 1003=I
217 131 1000=ID1*(N/2+1)
218 132 1003=I
219 133 1000=ID1*(N/2+1)
220 134 1003=I
221 135 1000=ID1*(N/2+1)
222 136 1003=I
223 137 1000=ID1*(N/2+1)
224 138 1003=I
225 139 1000=ID1*(N/2+1)
226 140 1003=I
227 141 1000=ID1*(N/2+1)
228 142 1003=I
229 143 1000=ID1*(N/2+1)
230 144 1003=I
231 145 1000=ID1*(N/2+1)
232 146 1003=I
233 147 1000=ID1*(N/2+1)
234 148 1003=I
235 149 1000=ID1*(N/2+1)
236 150 1003=I
237 151 1000=ID1*(N/2+1)
238 152 1003=I
239 153 1000=ID1*(N/2+1)
240 154 1003=I
241 155 1000=ID1*(N/2+1)
242 156 1003=I
243 157 1000=ID1*(N/2+1)
244 158 1003=I
245 159 1000=ID1*(N/2+1)
246 160 1003=I
247 161 1000=ID1*(N/2+1)
248 162 1003=I
249 163 1000=ID1*(N/2+1)
250 164 1003=I
251 165 1000=ID1*(N/2+1)
252 166 1003=I
253 167 1000=ID1*(N/2+1)
254 168 1003=I
255 169 1000=ID1*(N/2+1)
256 170 1003=I
257 171 1000=ID1*(N/2+1)
258 172 1003=I
259 173 1000=ID1*(N/2+1)
260 174 1003=I
261 175 1000=ID1*(N/2+1)
262 176 1003=I
263 177 1000=ID1*(N/2+1)
264 178 1003=I
265 179 1000=ID1*(N/2+1)
266 180 1003=I
267 181 1000=ID1*(N/2+1)
268 182 1003=I
269 183 1000=ID1*(N/2+1)
270 184 1003=I
271 185 1000=ID1*(N/2+1)
272 186 1003=I
273 187 1000=ID1*(N/2+1)
274 188 1003=I
275 189 1000=ID1*(N/2+1)
276 190 1003=I
277 191 1000=ID1*(N/2+1)
278 192 1003=I
279 193 1000=ID1*(N/2+1)
280 194 1003=I
281 195 1000=ID1*(N/2+1)
282 196 1003=I
283 197 1000=ID1*(N/2+1)
284 198 1003=I
285 199 1000=ID1*(N/2+1)
286 200 1003=I
287 201 1000=ID1*(N/2+1)
288 202 1003=I
289 203 1000=ID1*(N/2+1)
290 204 1003=I
291 205 1000=ID1*(N/2+1)
292 206 1003=I
293 207 1000=ID1*(N/2+1)
294 208 1003=I
295 209 1000=ID1*(N/2+1)
296 210 1003=I
297 211 1000=ID1*(N/2+1)
298 212 1003=I
299 213 1000=ID1*(N/2+1)
300 214 1003=I
301 215 1000=ID1*(N/2+1)
302 216 1003=I
303 217 1000=ID1*(N/2+1)
304 218 1003=I
305 219 1000=ID1*(N/2+1)
306 220 1003=I
307 221 1000=ID1*(N/2+1)
308 222 1003=I
309 223 1000=ID1*(N/2+1)
310 224 1003=I
311 225 1000=ID1*(N/2+1)
312 226 1003=I
313 227 1000=ID1*(N/2+1)
314 228 1003=I
315 229 1000=ID1*(N/2+1)
316 230 1003=I
317 231 1000=ID1*(N/2+1)
318 232 1003=I
319 233 1000=ID1*(N/2+1)
320 234 1003=I
321 235 1000=ID1*(N/2+1)
322 236 1003=I
323 237 1000=ID1*(N/2+1)
324 238 1003=I
325 239 1000=ID1*(N/2+1)
326 240 1003=I
327 241 1000=ID1*(N/2+1)
328 242 1003=I
329 243 1000=ID1*(N/2+1)
330 244 1003=I
331 245 1000=ID1*(N/2+1)
332 246 1003=I
333 247 1000=ID1*(N/2+1)
334 248 1003=I
335 249 1000=ID1*(N/2+1)
336 250 1003=I
337 251 1000=ID1*(N/2+1)
338 252 1003=I
339 253 1000=ID1*(N/2+1)
340 254 1003=I
341 255 1000=ID1*(N/2+1)
342 256 1003=I
343 257 1000=ID1*(N/2+1)
344 258 1003=I
345 259 1000=ID1*(N/2+1)
346 260 1003=I
347 261 1000=ID1*(N/2+1)
348 262 1003=I
349 263 1000=ID1*(N/2+1)
350 264 1003=I
351 265 1000=ID1*(N/2+1)
352 266 1003=I
353 267 1000=ID1*(N/2+1)
354 268 1003=I
355 269 1000=ID1*(N/2+1)
356 270 1003=I
357 271 1000=ID1*(N/2+1)
358 272 1003=I
359 273 1000=ID1*(N/2+1)
360 274 1003=I
361 275 1000=ID1*(N/2+1)
362 276 1003=I
363 277 1000=ID1*(N/2+1)
364 278 1003=I
365 279 1000=ID1*(N/2+1)
366 280 1003=I
367 281 1000=ID1*(N/2+1)
368 282 1003=I
369 283 1000=ID1*(N/2+1)
370 284 1003=I
371 285 1000=ID1*(N/2+1)
372 286 1003=I
373 287 1000=ID1*(N/2+1)
374 288 1003=I
375 289 1000=ID1*(N/2+1)
376 290 1003=I
377 291 1000=ID1*(N/2+1)
378 292 1003=I
379 293 1000=ID1*(N/2+1)
380 294 1003=I
381 295 1000=ID1*(N/2+1)
382 296 1003=I
383 297 1000=ID1*(N/2+1)
384 298 1003=I
385 299 1000=ID1*(N/2+1)
386 300 1003=I
387 301 1000=ID1*(N/2+1)
388 302 1003=I
389 303 1000=ID1*(N/2+1)
390 304 1003=I
391 305 1000=ID1*(N/2+1)
392 306 1003=I
393 307 1000=ID1*(N/2+1)
394 308 1003=I
395 309 1000=ID1*(N/2+1)
396 310 1003=I
397 311 1000=ID1*(N/2+1)
398 312 1003=I
399 313 1000=ID1*(N/2+1)
400 314 1003=I
401 315 1000=ID1*(N/2+1)
402 316 1003=I
403 317 1000=ID1*(N/2+1)
404 318 1003=I
405 319 1000=ID1*(N/2+1)
406 320 1003=I
407 321 1000=ID1*(N/2+1)
408 322 1003=I
409 323 1000=ID1*(N/2+1)
410 324 1003=I
411 325 1000=ID1*(N/2+1)
412 326 1003=I
413 327 1000=ID1*(N/2+1)
414 328 1003=I
415 329 1000=ID1*(N/2+1)
416 330 1003=I
417 331 1000=ID1*(N/2+1)
418 332 1003=I
419 333 1000=ID1*(N/2+1)
420 334 1003=I
421 335 1000=ID1*(N/2+1)
422 336 1003=I
423 337 1000=ID1*(N/2+1)
424 338 1003=I
425 339 1000=ID1*(N/2+1)
426 340 1003=I
427 341 1000=ID1*(N/2+1)
428 342 1003=I
429 343 1000=ID1*(N/2+1)
430 344 1003=I
431 345 1000=ID1*(N/2+1)
432 346 1003=I
433 347 1000=ID1*(N/2+1)
434 348 1003=I
435 349 1000=ID1*(N/2+1)
436 350 1003=I
437 351 1000=ID1*(N/2+1)
438 352 1003=I
439 353 1000=ID1*(N/2+1)
440 354 1003=I
441 355 1000=ID1*(N/2+1)
442 356 1003=I
443 357 1000=ID1*(N/2+1)
444 358 1003=I
445 359 1000=ID1*(N/2+1)
446 360 1003=I
447 361 1000=ID1*(N/2+1)
448 362 1003=I
449 363 1000=ID1*(N/2+1)
450 364 1003=I
451 365 1000=ID1*(N/2+1)
452 366 1003=I
453 367 1000=ID1*(N/2+1)
454 368 1003=I
455 369 1000=ID1*(N/2+1)
456 370 1003=I
457 371 1000=ID1*(N/2+1)
458 372 1003=I
459 373 1000=ID1*(N/2+1)
460 374 1003=I
461 375 1000=ID1*(N/2+1)
462 376 1003=I
463 377 1000=ID1*(N/2+1)
464 378 1003=I
465 379 1000=ID1*(N/2+1)
466 380 1003=I
467 381 1000=ID1*(N/2+1)
468 382 1003=I
469 383 1000=ID1*(N/2+1)
470 384 1003=I
471 385 1000=ID1*(N/2+1)
472 386 1003=I
473 387 1000=ID1*(N/2+1)
474 388 1003=I
475 389 1000=ID1*(N/2+1)
476 390 1003=I
477 391 1000=ID1*(N/2+1)
478 392 1003=I
479 393 1000=ID1*(N/2+1)
480 394 1003=I
481 395 1000=ID1*(N/2+1)
482 396 1003=I
483 397 1000=ID1*(N/2+1)
484 398 1003=I
485 399 1000=ID1*(N/2+1)
486 400 1003=I
487 401 1000=ID1*(N/2+1)
488 402 1003=I
489 403 1000=ID1*(N/2+1)
490 404 1003=I
491 405 1000=ID1*(N/2+1)
492 406 1003=I
493 407 1000=ID1*(N/2+1)
494 408 1003=I
495 409 1000=ID1*(N/2+1)
496 410 1003=I
497 411 1000=ID1*(N/2+1)
498 412 1003=I
499 413 1000=ID1*(N/2+1)
500 414 1003=I
501 415 1000=ID1*(N/2+1)
502 416 1003=I
503 417 1000=ID1*(N/2+1)
504 418 1003=I
505 419 1000=ID1*(N/2+1)
506 420 1003=I
507 421 1000=ID1*(N/2+1)
508 422 1003=I
509 423 1000=ID1*(N/2+1)
510 424 1003=I
511 425 1000=ID1*(N/2+1)
512 426 1003=I
513 427 1000=ID1*(N/2+1)
514 428 1003=I
515 429 1000=ID1*(N/2+1)
516 430 1003=I
517 431 1000=ID1*(N/2+1)
518 432 1003=I
519 433 1000=ID1*(N/2+1)
520 434 1003=I
521 435 1000=ID1*(N/2+1)
522 436 1003=I
523 437 1000=ID1*(N/2+1)
524 438 1003=I
525 439 1000=ID1*(N/2+1)
526 440 1003=I
527 441 1000=ID1*(N/2+1)
528 442 1003=I
529 443 1000=ID1*(N/2+1)
530 444 1003=I
531 445 1000=ID1*(N/2+1)
532 446 1003=I
533 447 1000=ID1*(N/2+1)
534 448 1003=I
535 449 1000=ID1*(N/2+1)
536 450 1003=I
537 451 1000=ID1*(N/2+1)
538 452 1003=I
539 453 1000=ID1*(N/2+1)
540 454 1003=I
541 455 1000=ID1*(N/2+1)
542 456 1003=I
543 457 1000=ID1*(N/2+1)
544 458 1003=I
545 459 1000=ID1*(N/2+1)
546 460 1003=I
547 461 1000=ID1*(N/2+1)
548 462 1003=I
549 463 1000=ID1*(N/2+1)
550 464 1003=I
551 465 1000=ID1*(N/2+1)
552 466 1003=I
553 467 1000=ID1*(N/2+1)
554 468 1003=I
555 469 1000=ID1*(N/2+1)
556 470 1003=I
557 471 1000=ID1*(N/2+1)
558 472 1003=I
559 473 1000=ID1*(N/2+1)
560 474 1003=I
561 475 1000=ID1*(N/2+1)
562 476 1003=I
563 477 1000=ID1*(N/2+1)
564 478 1003=I
565 479 1000=ID1*(N/2+1)
566 480 1003=I
567 481 1000=ID1*(N/2+1)
568 482 1003=I
569 483 1000=ID1*(N/2+1)
570 484 1003=I
571 485 1000=ID1*(N/2+1)
572 486 1003=I
573 487 1000=ID1*(N/2+1)
574 488 1003=I
575 489 1000=ID1*(N/2+1)
576 490 1003=I
577 491 1000=ID1*(N/2+1)
578 492 1003=I
579 493 1000=ID1*(N/2+1)
580 494 1003=I
581 495 1000=ID1*(N/2+1)
582 496 1003=I
583 497 1000=ID1*(N/2+1)
584 498 1003=I
585 499 1000=ID1*(N/2+1)
586 500 1003=I
587 501 1000=ID1*(N/2+1)
588 502 1003=I
589 503 1000=ID1*(N/2+1)
590 504 1003=I
591 505 1000=ID1*(N/2+1)
592 506 1003=I
593 507 1000=ID1*(N/2+1)
594 508 1003=I
595 509 1000=ID1*(N/2+1)
596 510 1003=I
597 511 1000=ID1*(N/2+1)
598 512 1003=I
599 513 1000=ID1*(N/2+1)
600 514 1003=I
601 515 1000=ID1*(N/2+1)
602 516 1003=I
603 517 1000=ID1*(N/2+1)
604 518 1003=I
605 519 1000=ID1*(N/2+1)
606 520 1003=I
607 521 1000=ID1*(N/2+1)
608 522 1003=I
609 523 1000=ID1*(N/2+1)
610 524 1003=I
611 525 1000=ID1*(N/2+1)
612 526 1003=I
613 527 1000=ID1*(N/2+1)
614 528 1003=I
615 529 1000=ID1*(N/2+1)
616 530 1003=I
617 531 1000=ID1*(N/2+1)
618 532 1003=I
619 533 1000=ID1*(N/2+1)
620 534 1003=I
621 535 1000=ID1*(N/2+1)
622 536 1003=I
623 537 1000=ID1*(N/2+1)
624 538 1003=I
625 539 1000=ID1*(N/2+1)
626 540 1003=I
627 541 1000=ID1*(N/2+1)
628 542 1003=I
629 543 1000=ID1*(N/2+1)
630 544 1003=I
631 545 1000=ID1*(N/2+1)
632 546 1003=I
633 547 1000=ID1*(N/2+1)
634 548 1003=I
635 549 1000=ID1*(N/2+1)
636 550 1003=I
637 551 1000=ID1*(N/2+1)
638 552 1003=I
639 553 1000=ID1*(N/2+1)
640 554 1003=I
641 555 1000=ID1*(N/2+1)
642 556 1003=I
643 557 1000=ID1*(N/2+1)
644 558 1003=I
645 559 1000=ID1*(N/2+1)
646 560 1003=I
647 561 1000=ID1*(N/2+1)
648 562 1003=I
649 563 1000=ID1*(N/2+1)
650 564 1003=I
651 565 1000=ID1*(N/2+1)
652 566 1003=I
653 567 1000=ID1*(N/2+1)
654 568 1003=I
655 569 1000=ID1*(N/2+1)
656 570 1003=I
657 571 1000=ID1*(N/2+1)
658 572 1003=I
659 573 1000=ID1*(N/2+1)
660 574 1003=I
661 575 1000=ID1*(N/2+1)
662 576 1003=I
663 577 1000=ID1*(N/2+1)
664 578 1003=I
665 579 1000=ID1*(N/2+1)
666 580 1003=I
667 581 1000=ID1*(N/2+1)
668 582 1003=I
669 583 1000=ID1*(N/2+1)
670 584 1003=I
671 585 1000=ID1*(N/2+1)
672 586 1003=I
673 587 1000=ID1*(N/2+1)
674 588 1003=I
675 589 1000=ID1*(N/2+1)
676 590 1003=I
677 591 1000=ID1*(N/2+1)
678 592 1003=I
679 593 1000=ID1*(N/2+1)
680 594 1003=I
681 595 1000=ID1*(N/2+1)
682 596 1003=I
683 597 1000=ID1*(N/2+1)
684 598 1003=I
685 599 1000=ID1*(N/2+1)
686 600 1003=I
687 601 1000=ID1*(N/2+1)
688 602 1003=I
689 603 1000=ID1*(N/2+1)
690 604 1003=I
691 605 1000=ID1*(N/2+1)
692 606 1003=I
693 607 1000=ID1*(N/2+1)
694 608 1003=I
695 609 1000=ID1*(N/2+1)
696 610 1003=I
697 611 1000=ID1*(N/2+1)
698 612 1003=I
699 613 1000=ID1*(N/2+1)
700 614 1003=I
701 615 1000=ID1*(N/2+1)
702 616 1003=I
703 617 1000=ID1*(N/2+1)
704 618 1003=I
705 619 1000=ID1*(N/2+1)
706 620 1003=I
707 621 1000=ID1*(N/2+1)
708 622 1003=I
709 623 1000=ID1*(N/2+1)
710 624 1003=I
711 625 1000=ID1*(N/2+1)
712 626 1003=I
713 627 1000=ID1*(N/2+1)
714 628 1003=I
715 629 1000=ID1*(N/2+1)
716 630 1003=I
717 631 1000=ID1*(N/2+1)
718 632 1003=I
719 633 1000=ID1*(N/2+1)
720 634 1003=I
721 635 1000=ID1*(N/2+1)
722 636 1003=I
723 637 1000=ID1*(N/2+1)
724 638 1003=I
725 639 1000=ID1*(N/2+1)
726 640 1003=I
727 641 1000=ID1*(N/2+1)
728 642 1003=I
729 643 1000=ID1*(N/2+1)
730 644 1003=I
731 645 1000=ID1*(N/2+1)
732 646 1003=I
733 647 1000=ID1*(N/2+1)
734 648 1003=I
735 649 1000=ID1*(N/2+1)
736 650 1003=I
737 651 1000=ID1*(N/2+1)
738 652 1003=I
739 653 1000=ID1*(N/2+1)
740 654 1003=I
741 655 1000=ID1*(N/2+1)
742 656 1003=I
743 657 1000=ID1*(N/2+1)
744 658 1003=I
745 659 1000=ID1*(N/2+1)
746 660 1003=I
747 661 1000=ID1*(N/2+1)
748 662 1003=I
749 663 1000=ID1*(N/2+1)
750 664 1003=I
751 665 1000=ID1*(N/2+1)
752 666 1003=I
753 667 1000=ID1*(N/2+1)
754 668 1003=I
755 669 1000=ID1*(N/2+1)
756 670 1003=I
757 671 1000=ID1*(N/2+1)
758 672 1003=I
759 673 1000=ID1*(N/2+1)
760 674 1003=I
761 675 1000=ID1*(N/2+1)
762 676 1003=I
763 677 1000=ID1*(N
```



```

FFTT0001
FFTT0002
FFTT0003
FFTT0004
FFTT0005
FFTT0006
FFTT0007
FFTT0008
FFTT0009
FFTT0010
FFTT0011
FFTT0012
FFTT0013
FFTT0014
FFTT0015
FFTT0016
FFTT0017
FFTT0018
FFTT0019
FFTT0020

```

```

DATA(I)=DATA(J)
DATA(I+1)=-DATA(J+1)
J=J+1
J=J+1
DATA(I)=DATA(J)
DATA(I+1)=-DATA(J+1)
J=J+1

```

END OF LOOP ON EACH DIMENSION

```

NO END
NO END
NO END
NO END

```

CARD NO. SEVERITY DETAILS DIAGNOSIS OF PROBLEM

```

40. I DAT: ARRAY REFERENCE OUTSIDE DIMENSION BOUNDS.
49. I DAT: ARRAY REFERENCE OUTSIDE DIMENSION BOUNDS.

```

97

SYMBOLIC REFERENCE MAP (R=1)

ENTRY POINTS
3 FOUJST

VARIABLES	ON	TYPE	DECLARATION	LOC	TYPE	DECLARATION
1326 DATA		REAL		1027	REAL	
1327 DIF		REAL		1417	REAL	
1408 ACAS		INTEGER		1413	INTEGER	
1412 IDIM		INTEGER		1411	INTEGER	
1413 IFC		INTEGER		1473	INTEGER	
1413 IFS		INTEGER		1524	INTEGER	
1514 IMAY		INTEGER	IMAY	1413	INTEGER	
1415 IPI		INTEGER		1425	INTEGER	
1416 IPI		INTEGER		1424	INTEGER	
1417 I1		INTEGER		1434	INTEGER	
1421 I1NS		INTEGER		1531	INTEGER	
1421 I2NX		INTEGER		1515	INTEGER	
1425 J		INTEGER		1511	INTEGER	
1425 JMIN		INTEGER		1512	INTEGER	
1426 J1CN1		INTEGER		1513	INTEGER	
1426 J1CN2		INTEGER		1514	INTEGER	
1426 J1CN3		INTEGER		1515	INTEGER	
1426 J1CN4		INTEGER		1516	INTEGER	
1426 J1CN5		INTEGER		1517	INTEGER	
1426 J1CN6		INTEGER		1518	INTEGER	
1426 J1CN7		INTEGER		1519	INTEGER	
1426 J1CN8		INTEGER		1520	INTEGER	
1426 J1CN9		INTEGER		1521	INTEGER	
1426 J1CN10		INTEGER		1522	INTEGER	
1426 KCC1		INTEGER		1523	INTEGER	
1426 KMIN		INTEGER		1524	INTEGER	

F.P.

F.P.

VITA

James Singletery Jr. was born on November 4, 1955 in Lackawanna, New York. He graduated from Lackawanna Senior High School in June 1973 and entered the United States Air Force Academy that same month. In June of 1977, he graduated from the Air Force Academy with a Bachelor of Science degree in Electrical Engineering and a commission in the United States Air Force. From July 1977 to June 1979, he served as a telemetry developmental engineer with the 4950th Test Wing at Wright-Patterson Air Force Base, Ohio. In June 1979, First Lieutenant James Singletery Jr. was assigned to the Air Force Institute of Technology to pursue a Master's of Science Degree in Electrical Engineering (Electro-Optics). As a result of graduate work done at night during his assignment with the Test Wing, he earned a Master's of Science Degree in Management Science in April 1980 from the University of Dayton. Lt. Singletery is also a member of the Eta Kappa Nu Society.

Permanent address: 11 Clark St.
Lackawanna, New York 14218

UNCLASSIFIED

SECURITY CLASSIFICATION OF THIS PAGE (When Data Entered)

REPORT DOCUMENTATION PAGE		READ INSTRUCTIONS BEFORE COMPLETING FORM
1. REPORT NUMBER AFIT/GEO/EE/80D-12	2. GOVT ACCESSION NO. AD A100870	3. RECIPIENT'S CATALOG NUMBER
4. TITLE (and Subtitle) ADAPTIVE LASER POINTING AND TRACKING PROBLEM		5. TYPE OF REPORT & PERIOD COVERED MS Thesis
7. AUTHOR(s) James Singletery Jr., 1st Lt.		6. PERFORMING ORG. REPORT NUMBER
9. PERFORMING ORGANIZATION NAME AND ADDRESS Air Force Institute of Technology (AFIT-EN) Wright-Patterson AFB, Ohio 45433		8. CONTRACT OR GRANT NUMBER(s)
11. CONTROLLING OFFICE NAME AND ADDRESS Air Force Weapons Laboratory/ALO Kirtland AFB, NM 87117		10. PROGRAM ELEMENT, PROJECT, TASK AREA & WORK UNIT NUMBERS
14. MONITORING AGENCY NAME & ADDRESS (if different from Controlling Office)		12. REPORT DATE December, 1980
		13. NUMBER OF PAGES 108
		15. SECURITY CLASS. (of this report) Unclassified
		15a. DECLASSIFICATION DOWNGRADING SCHEDULE
16. DISTRIBUTION STATEMENT (of this Report) Approved for public release; distribution unlimited		
17. DISTRIBUTION STATEMENT (of the abstract entered in Block 20, if different from Report)		
18. SUPPLEMENTARY NOTES Approved for public release; IAW AFR 190-17 <i>Frederic C. Lynch</i> Frederic C. Lynch, Major, USAF Director of Public Affairs, AFIT 16 JUN 1981		
19. KEY WORDS (Continue on reverse side if necessary and identify by block number) Kalman Filter Pattern Recognition Fast Fourier Transform		
20. ABSTRACT (Continue on reverse side if necessary and identify by block number) Although a number of the major objectives that were established at the outset of this project were not met, a number of milestones were realized. The digital implementation of a negating phase shift that operates perfectly under ideal conditions was a major accomplishment. The establishment of a zero level of 10^{-8} was also significant. The incorporation of the exponential smoothing technique to minimize the effect of measurement noise was important since it uncovered a possible connection between the size of the target image and its		

DD FORM 1473 EDITION OF 1 NOV 65 IS OBSOLETE

UNCLASSIFIED
SECURITY CLASSIFICATION OF THIS PAGE (When Data Entered)

20. ABSTRACT

performance throughout the pattern recognition process. However, the major obstacle that surfaced during the execution of this project was a filter divergence problem. It has been proposed that this problem can be solved by implementing the Fourier transform derivative property instead of the forward-backward difference method to compute the spatial derivative of the non-linear h function.